Final Report

submitted to

NATIONAL AERONAUTICS AND SPACE ADMINISTRATION
GEORGE C. MARSHALL SPACE FLIGHT CENTER, ALABAMA 35812

June 7, 1993

for Contract NAS8 - 38609

Delivery Order 15

entitled

MATERIAL CHARACTERIZATION AND MODELING WITH SHEAROGRAPHY

by

Gary L. Workman Ph.D.
Principal Investigator
and
Virginia Callahan
Mechanical Engineering Student

Materials Processing Laboratory
Center for Automation & Robotics
University of Alabama in Huntsville
Huntsville, Alabama 35899

TABLE OF CONTENTS

1.0 INTRODUCTION

The use of optical techniques for nondestructive evaluation (NDE) of structural materials continues to expand as the range of materials and the overall capabilities of the various techniques increase. The diversity of optical NDE techniques allows for evaluation of many types of materials. For instance, one of the older techniques, the use of polarized light for detection of stresses in optical glass, has been used for a century of more by the glass-blowing industry. Optical techniques have the general advantage of being non-contact and in many cases, can provide a full image of a reasonably large area of interest for inspection purposes. For the purpose of using optical techniques for NDE, a major distinction can be made between coherent and non-coherent methods. Prior to the development of lasers, most of the information gained by optical inspection was either visual inspection, infra-red, or moire patterns. As shown in Table 1, coherent laser sources adds some new capability and much more sensitivity to defect characterization. More recent advances in coherent laser sources, which provides an extremely sensitive approach to measuring structural parameters such as displacements, enables optical techniques to display even better sensitivity than previous technology was able to accomplish.

Table 1. Optical NDE Techniques

Non-coherent	Coherent
Photoelasticity	Holography
Moire Imaging	Speckle Interferometry
Thermal Imaging	2-D Image Correlation
	Shearography

All the optical techniques which use coherent light typically use gaseous lasers such as helium-neon and or argon for fairly long coherence length. The solid state lasers, such as ruby or Nd-YAG, provide much more energy per pulse than the cw lasers and are used for very fast, real-time applications, particularly for double exposure holography.

As our understanding of structural properties of materials improves, it has become worthwhile developing the capability to model NDE experiments in such a way that experimental results can be interpreted properly.

2.0 PRINCIPLES OF SHEAROGRAPHY

Historically, shearography has evolved from the original work of Leendertz in the early 1970's, who was developing methodology to measure bending moments of structures under loading conditions.[1,2] Most of the research being performed at that time was concentrated in applying the new and emerging capabilities of holography and its spin-off technologies, one of which was speckle interferometry. The optical arrangement chosen at that time to provide surface displacement information was that of a Michelson interferometer, with the ability to tilt the angle between mirrors, M1 and M2, in Figure 1.

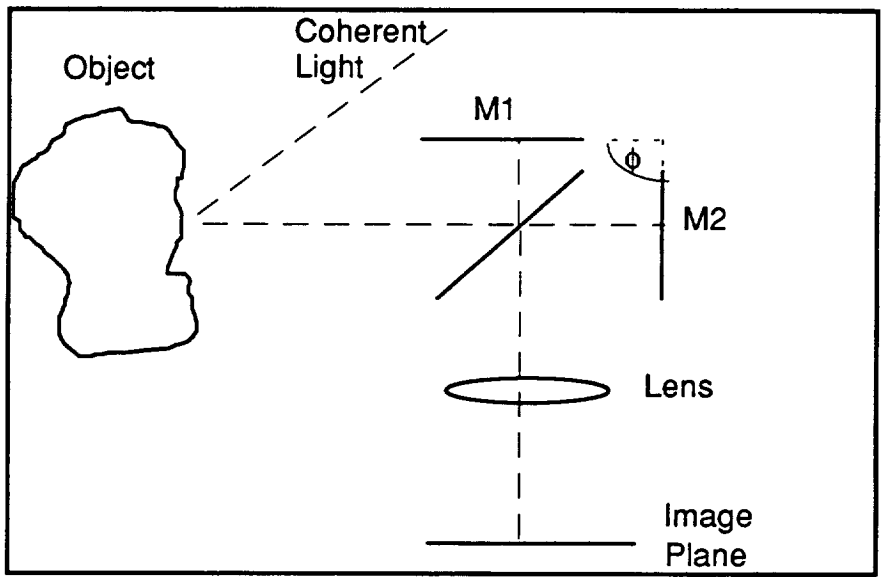

Figure 1. Schematic showing the Michelson Interferometer arrangement used by Leendertz.

The key to being able to measure in plane displacements was achieved by forming two identical images of the surface with a lateral shift between them. Hence by varying angle ϕ in Figure 1, sheared images in the plane of the figure are obtained. To determine displacements in the plane perpendicular to the figure, shearing (and tilt of the mirrors) has to be performed in the plane perpendicular to this page.

The mathematical framework for the modified Michelson inferometer is given in the original work performed by Leendertz [1,2] and Boone [6]. Following the nomenclature of Boone, one arrives at fringe pattern in the image plane given by:

$$\text{intensity maxima occurs when } \frac{\partial\omega(x,y)}{\partial x} = \frac{k\lambda}{2\delta} \quad \text{for } |k| = 0,1,2,,,\text{etc}$$

and

$$\text{intensity minima occurs when } \frac{\partial\omega(x,y)}{\partial x} = \frac{(k+1/2)\lambda}{2\delta} \quad \text{for } |k| = 0,1,2,,,\text{etc}$$

where $\partial\omega(x,y)$ represents the deflection in the (x,y) plane

∂x is the change along a principal axis in the surface of the sample

k is an order number of the fringe formation

λ is the wavelength of the coherent light source

δ is the shift of the sheared image in the image plane.

Boone's work also included experiments and theoretical foundation for determining a sensitivity analysis for his experimental arrangement. His arguments showed that experimental errors could be associated with:

error on $\delta \cong \lambda/2\delta$ or about 1%

error in determining centers of fringes $\cong \lambda/20\delta$ or about 0.1%

Note that $\frac{\partial\omega(x,y)}{\partial x}$ is actually one of the two strain components measured along the two principal directions of the material surface. For example, the normal strain components ε_{xx} , ε_{xx} and the tangential strain ε_{xx} are related to the deflection (w(x,y) of a thin plate of thickness h by the following expressions:[11]

$$\varepsilon_{xx} = \frac{h}{2}\frac{\partial\omega^2(x,y)}{\partial^2 x}$$

$$\varepsilon_{yy} = \frac{h}{2}\frac{\partial\omega^2(x,y)}{\partial^2 y}$$

$$\gamma_{xy} = h\frac{\partial\omega^2(x,y)}{\partial\, xy}$$

This fringe information then allows direct observation of the strain components of a sample under load. The current shearography system being used at Marshall space Flight Center has been developed along the modified Michelson interferometer and thus fits into this category in terms of the experiment capability of the instrument.

Since shearography can be considered a speckle interferometric technique for directly measuring displacement gradients on the surface of a material.[3-5] An image of the object, which is illuminated with a coherent light source, is acquired with an optical path difference occurring in one half of the light rays being transmitted to the image plane as shown in Figure 2. Note that this arrangement is an alternate methodology for the generation of sheared images. The active element for the shearing is the glass wedge which is located in the iris plane of the lens assembly. When rays from the coherent light source are scattered from an object point P0(x,y), the effect of the wedge is to map into the image plane two points, P1 and P2. Note that without the wedge then only one point would be imaged in the image plane for each point in the object plane.

Figure 2. Schematic of a shearography measurement system.

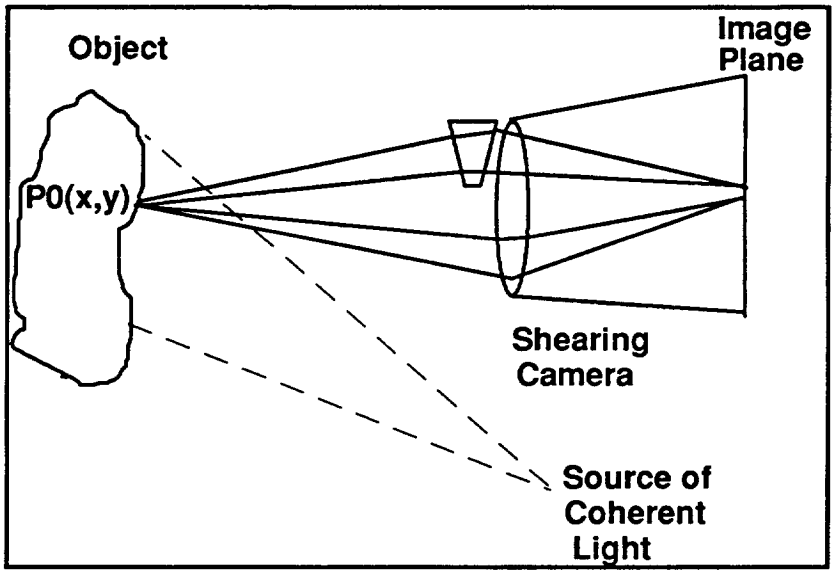

The result is a pair of laterally sheared images in the image plane, which produces a random interference or speckle pattern. When the object then becomes deformed due to some loading condition, the speckle pattern changes and superposition of the speckle pattern from deformed

and undeformed surface regions then yields a fringe pattern depicting the surface displacement gradient of the deformed object.

Y. Y. Hung has been the chief advocate for the latter of these two techniques.[3,4] The optical alignment is more easily accomplished, although optimization of the fringe separation and contrast has not been developed as thoroughly as that of the modified Michelson interferometer approach.[11] The expression developed for the optical arrangement using a wedge lens element is given by:

$$\Delta = \frac{2\pi}{\lambda}\left[A\frac{\partial u}{\partial x} + B\frac{\partial v}{\partial x} + C\frac{\partial w}{\partial x}\right]\partial x \quad \text{for the shearing direction in the x direction}$$

In this expression (u,v,w) represents the displacement vector of the point (x,y); A, B, C are related to the position of the illumination point and the camera position relative to the sample surface. Should the shearing direction be in the y direction then a similar relation holds for ∂y's replacing the ∂x's.

Using the above relation it is seen that three measurements with three different illumination angles are needed in order to obtain three displacement derivatives. For a normal illumination and viewing, with the camera separation large compared to sample size, then the relationship simplifies to:

$$\Delta = \frac{4\pi}{\lambda}(\partial x)\bullet\frac{\partial w}{\partial x} \quad \text{for the x direction and } \Delta = \frac{4\pi}{\lambda}(\partial y)\bullet\frac{\partial w}{\partial y} \quad \text{for the y direction.}$$

These equations show that the observed fringes are whole field representations of the loci $\frac{\partial w}{\partial x}$ and $\frac{\partial w}{\partial y}$. The measurement sensitivity of the method has not been presented in the literature survey obtained so far. It is apparent that the optical setup does provide an optimization requirement for both the fringe separation and for the contrast ration. An error analysis, much along the arguments presented by Boone, appear to be needed for the technique to become more quantitative.

3.0 ANSYS MODELS

Due the lack of an accurate and quantitative foundation for the strain measurements obtained in shearography, there seems to be a need for a numerical methodology to substantiate the shearographic observations obtained with commercial equipment. Therefore we have worked with one of the available finite element packages to determine how easily these packages can adapt to substantiating measurements such as derived from shearographic measurements.

3.1 Summary of ANSYS

ANSYS is a general purpose finite element analysis (FEA) program. ANSYS is used for solving complex engineering problems that would otherwise be very time consuming or impossible to solve. The example problems presented in this paper were not difficult to solve by hand calculations; but, the solutions were very time consuming. However, with the use of ANSYS, obtaining the solutions was greatly simplified.

Included in the different types of analyses which ANSYS offers are static, dynamic, mode frequency, full harmonic response, and heat transfer. Because many NDE tests require that the fixed test object is stressed through an applied force or applied heat, only the static and heat transfer analyses were utilized for this project.

Programming in ANSYS consists of the following three phases: 1) the preprocessing phase, 2) the solution phase, and 3) the post-processing phase.

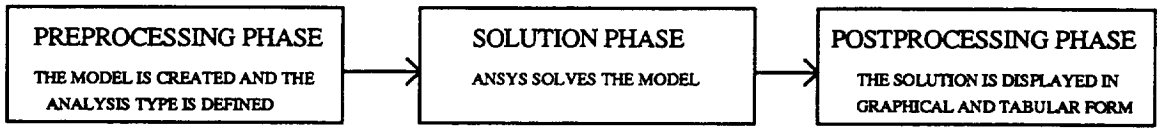

The finite element model is created during the preprocessing phase. First, the element type is defined. ANSYS offers 99 different pre-defined element types from which to chose. The element types are assigned a number, n, and referred to as stif n. Choosing the element type is one of the most critical decisions in the finite element design. Each element has a list of assumptions and restrictions which must be fully understood by the user for accurate results. Each element type has a number of options concerning the solution of the model and printout options. Some elements also include "real constants" which must be input by the user. The number of real constants and the values of these constants depend on the element type.

The analysis type must also be defined. ANSYS offers 8 different analysis types with various options for each analysis type. After the element type and analysis type have been defined, the geometry of the model is created through either nodal or mesh analysis. Nodal analysis involves first generating a node pattern in the shape of the desired model.

From these nodes the elements can then be generated based on the chosen element type. Mesh analysis is performed by defining keypoints and generating lines, areas, and volumes in the desired shape. The size of the element is then chosen and the mesh command is issued. The elements are automatically generated by ANSYS.

After the model is generated, the constraints and loads are applied. This is done using various ANSYS commands. The model is then saved and ready to be solved. The solution phase is completed by ANSYS with the use of the /INPUT,27 command. After the solution phase is complete, the results can be displayed in graphical or tabular form during the post-processing phase.

For this project, the following four ANSYS element types were used: 1) the stif 42 element, 2) the stif 45 element, 3) the stif 55 element, and 4) the stif 91 element. Each of these elements has different required inputs, assumptions, and restrictions. A description of these elements is given in the following section.

3.1.1 Stif 42 Element

The stif 42 element is a 2-dimensional isoparametric solid element with four nodal points as seen in figure 3. This element is used for 2-dimensional modeling of solids. Temperatures and forces can be applied to any of the four nodal points. Likewise, pressures can be applied to any of the faces.

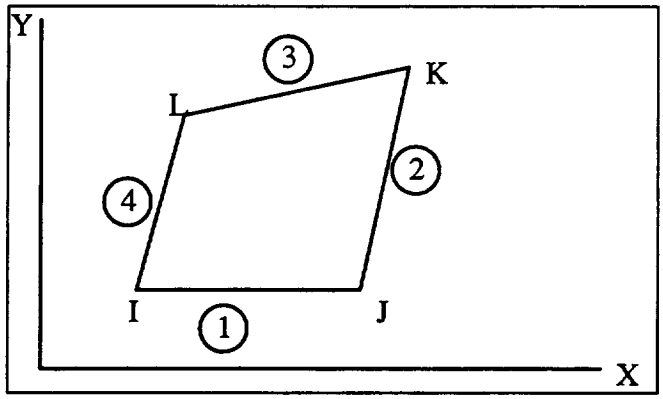

Figure 3. ANSYS Stif 42 Element

The stif 42 element has the following assumptions and restrictions:

1. The area of the element must be positive.
2. The element must lie in a global X-Y coordinate plane as shown in figure 3.

3.1.2 Stif 45 Element

The stif 45 element is a 3-dimensional isoparametric solid with eight nodal points as shown is figure 4. This element is used for 3-dimensional modeling of solids. Forces can be applied to the eight nodal points. Similarly, pressures can be applied to any of the six element faces.

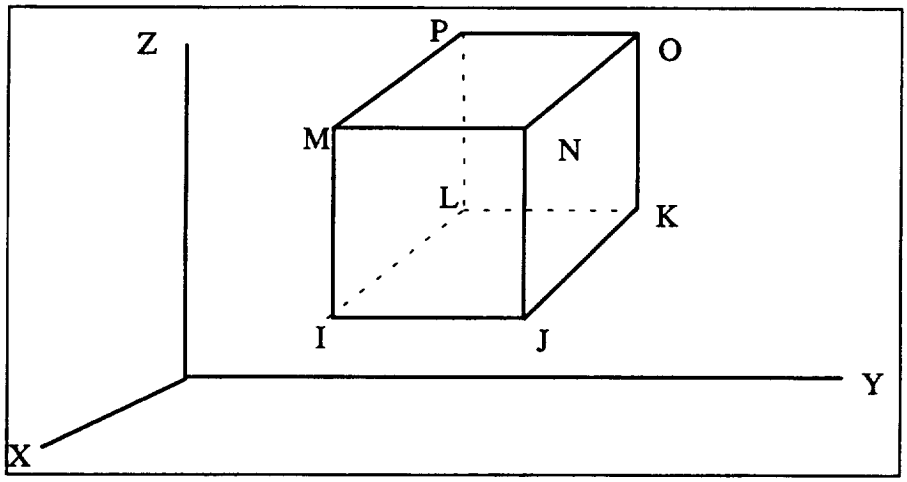

Figure 4. ANSYS Stif 45 Element

The stif 45 element has the following assumptions and restrictions according to ANSYS:

1. Orthotropic material directions correspond to the element coordinate directions.
2. Zero volume elements are not allowed.
3. The element may not be twisted such that the element has two separate volumes.
4. All elements must have eight nodes.

3.1.3 Stif 55 Element

The stif 55 element is a two-dimensional isoparametric thermal solid with four nodal points as shown in figure 5. This element is useful for two-dimensional heat transfer analyses, both steady-state and transient. Temperatures can be applied to the nodal points while convection can be applied to the faces.

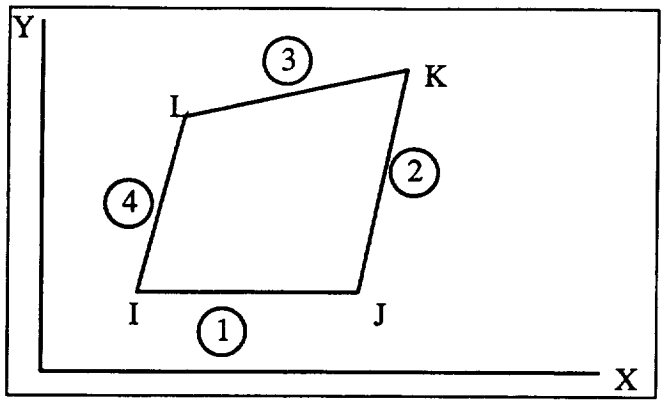

Figure 5. ANSYS Stif 55 Element

The stif 55 element has the following assumptions and restrictions according to ANSYS:

1. The element cannot have a negative or zero area.
2. The element must lie in the X-Y plane.
3. The specific heat is evaluated at each integration point to allow for abrupt changes within a coarse grid of elements.

3.1.4 Stif 91 Element

The stif 91 element is an eight node layered shell element as seen in figure 6. This element type is useful for modeling composite materials. This element type allows a maximum of 16 different material layers to be input.

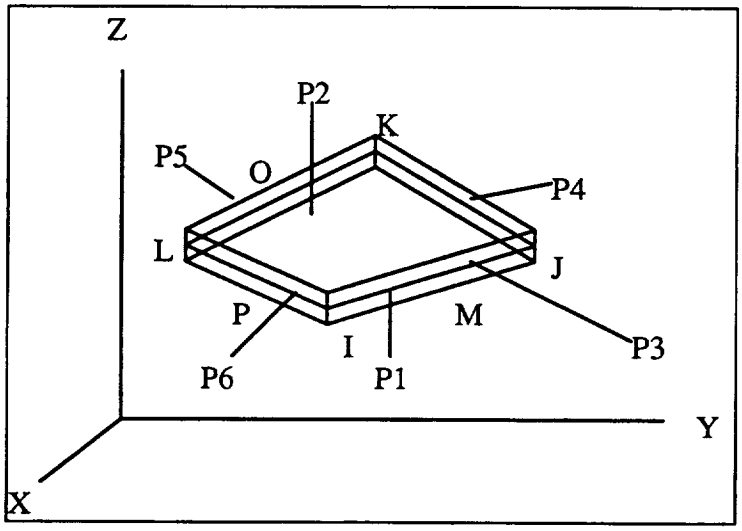

Figure 6. ANSYS Stif 91 Element

The stif 91 element is defined by eight nodal points. The thickness and angle orientation for each layer is defined with the use of real constants. The element can be loaded with pressures and/or temperatures. Elastic properties for the composite must be input for stress analysis and thermal properties must be input for heat transfer analyses.

The stif 91 element has the following assumptions and restrictions according to ANSYS:

1. Zero area elements are not allowed.
2. Zero thickness layers or layers tapering down to a zero thickness is not allowed.
3. All nodes are assumed to be located at the mid-thickness of the elements.
4. No slippage between the element layers can occur; thus, a composite with a debond cannot be modeled using this element type.
5. Shear deflections are included in the element; however, normals to the center plane are assumed to remain straight after deformation.
6. The stress varies linearly through the thickness of each layer.
7. Interlaminar transverse shear stresses are computed at the centroid of the element and may not be accurate along the element boundaries.
8. The thickness of each layer is assumed to vary linearly over the area of the layer.

3.2 Comparisons with Other Work

In order to feel comfortable with the results obtained from the finite element analysis, two textbook examples with known solutions were solved using ANSYS. In each case the ANSYS solution was compared to the known solution. These examples were included to verify the ANSYS models and to establish the credibility of the ANSYS user's programming abilities.

3.2.1 Heat Transfer Example

Many NDE techniques often use heat to stress the test object. For this reason, a simple heat transfer example with a known solution was solved using ANSYS to help verify the ANSYS models.

Problem Statement: A large industrial furnace is supported on a long column of fireclay brick, which is 1 m by 1m on a side. During steady state operation, installation is such that three surfaces of the column are maintained at 500 K while the remaining surface is exposed to an airstream for which T_∞=300 K and h=10 W/m^{2}K, as shown in figure 7.

Using the matrix inversion method with a grid of $\Delta x=\Delta y=.25$m, determine the airstream temperature per unit length of column.

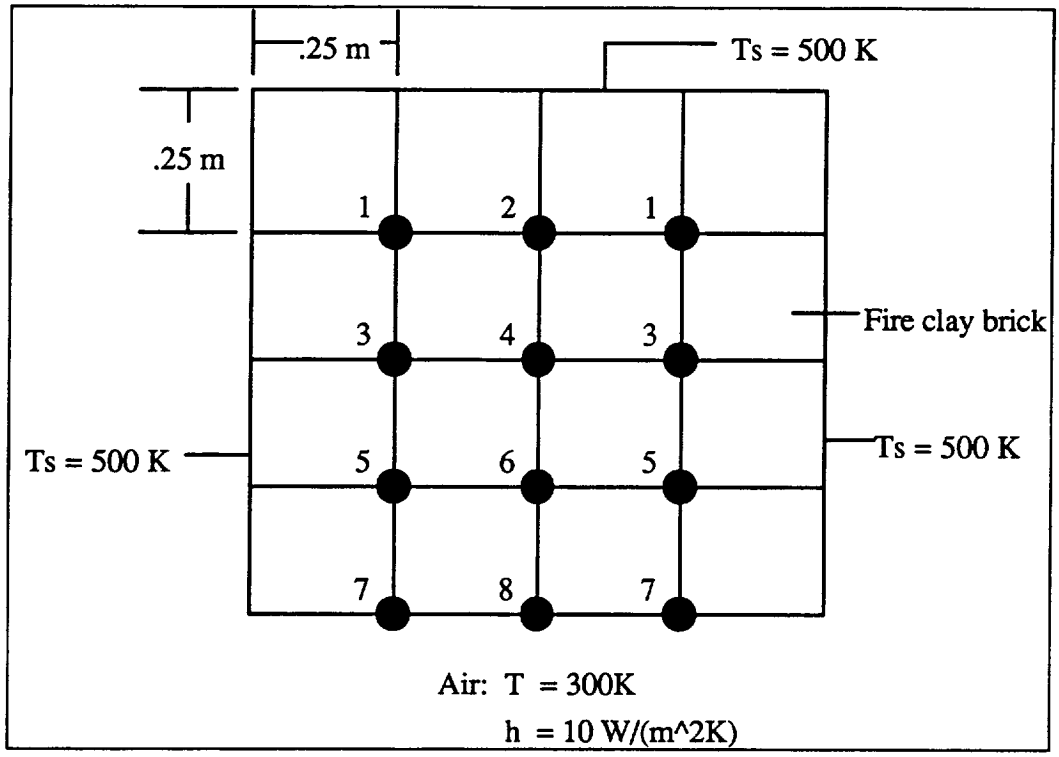

Figure 7. Schematic of Heat Transfer Problem

Textbook Solution:

A summary of the textbook solution is found in table 2. The complete textbook solution can be found in reference 15 pages 152-155.

ANSYS Solution:

This problem was modeled using the stif 55 element which is a two-dimensional isoparametric thermal solid. The material properties for the fireclay brick were input as well as the boundary conditions. The ANSYS model consisted of 16 .25m x .25m elements. The temperature distribution plot can be found in appendix 1.

Results:

Table 2. Heat Transfer Results- A Comparison of the ANSYS Results to the Textbook Results							
Final Answers							
T_1(K)	T_2(K)	T_3(K)	T_4(K)	T_5(K)	T_6(K)	T_7(K)	T_8(K)
489.3	485.2	472.1	462.0	437.0	418.7	357.0	339.1
ANSYS Final Answers							
T_1(K)	T_2(K)	T_3(K)	T_4(K)	T_5(K)	T_6(K)	T_7(K)	T_8(K)
491.2	487.5	475.8	465.9	443.8	418.2	350.6	339.7
Percent Difference of Textbook Results to ANSYS Results							
T_1	T_2	T_3	T_4	T_5	T_6	T_7	T_8
0.39%	0.47%	0.78%	0.84%	1.56%	0.13%	1.79%	0.18%

Discussion of Results:

It can be seen from the previous table that the results from the ANSYS solution are very similar to the results obtained from the textbook solution. The discrepancy between the two sets of results is probably due to the number of significant figures used in each of the solutions.

3.2.2 Composite Displacement Example

Composites are being increasingly used in aerospace applications. For this reason a stress analysis example involving a composite material was chosen to show that ANSYS is capable of solving problems involving complex materials such as composites.

Problem Statement: A rectangular specimen, with the dimensions 250mm x 20mm x 2mm is tested in uniaxial tension. Predict the load elongation curve for the specimen if the grips are initially 200mm apart. Assume that the laminae fail according to the maximum stress theory and that all the elastic constants of a lamina become zero when it fails.

Given: $E_L = 40$ GPa $G_{LT} = 4$ GPa stacking sequence: $[0/+45/-45/90]_S$
$E_T = 10$ GPa $\nu_{LT} = 0.285$

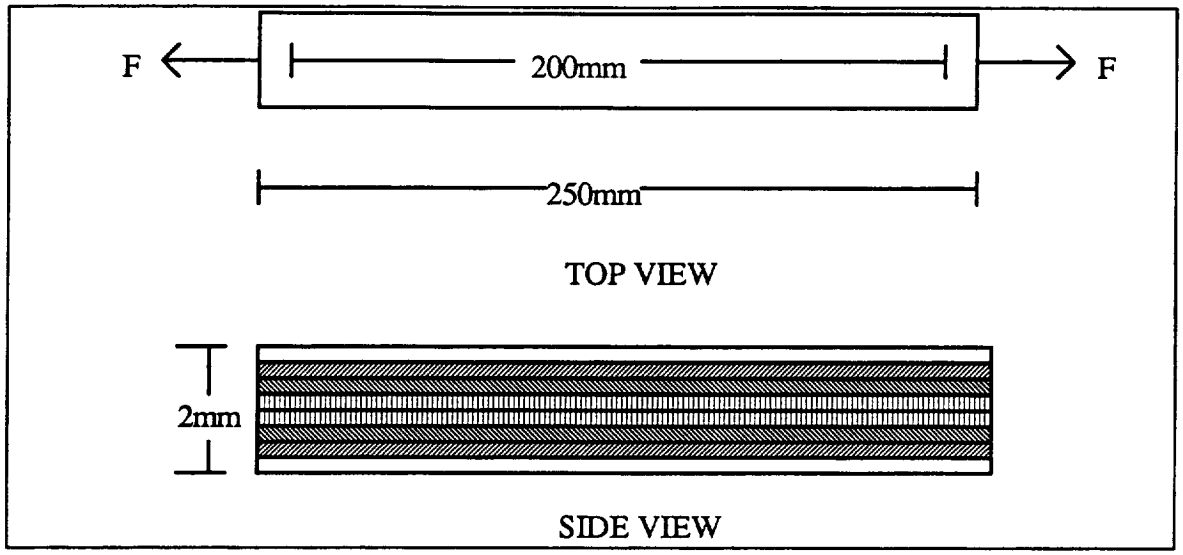

Figure 8. Schematic of Composite Example

Textbook Solution:

A summary of the textbook solution is found in table 4. The complete solution can be found in reference 14 pages 223-228.

ANSYS Solution:

The ANSYS solution for this problem was modeled using the composite element type, stif 91. The ply thickness and stacking sequence previously stated for the textbook solution were used and input into the code as real constants.

The elasticity constants stated in the original problem had to be converted to the proper engineering constants for the ANSYS program. This was accomplished through a series of equations found in appendix 7. The material properties for each layer vary according to the fiber orientation angle for each ply; therefore, each ply with its particular fiber orientation was treated as a different material. Table 3 shows the transformed engineering constants.

The boundary conditions in the problem had to be slightly altered to perform a static analysis using ANSYS. These modifications can be seen in figure 9.

Table 3. Transformed Material Properties for use with ANSYS

Θ	E_x (Pa)	E_y (Pa)	G_{xy} (Pa)	ν_{xy}
0	40E9	10E9	4E9	.285
+45	11.09E9	11.08E9	7.18E9	.386
-45	11.09E9	11.08E9	7.18E9	.386
90	10E9	40E9	4E9	.0713

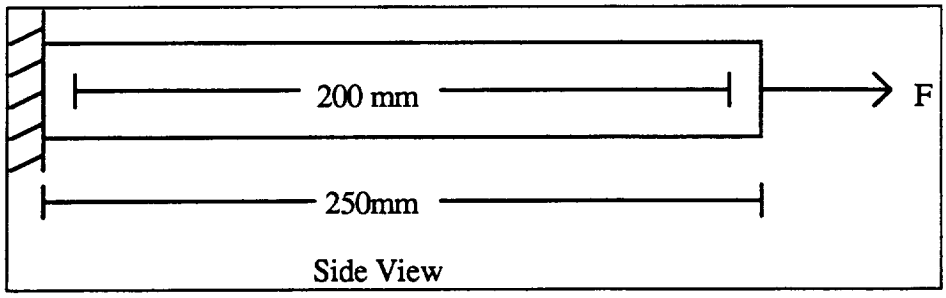

Figure 9- Schematic of Composite Example with Modified Boundary Conditions

Results:

Table 4. Solutions for the Composite Displacement Example- A comparison of the ANSYS Results to the Textbook Results			
Textbook Solution		**ANSYS Solution**	
Force (kN)	Displacement (mm)	Force (kN)	Displacement (mm)
0	0	0	0
2	.45	2	1.4
4	1.1	4	2.8
6	2.2	6	4.2
8	3.2	8	5.6
10	4.5	10	7.0
12	5.5	12	8.4

Discussion of Results:

The discrepancy in the textbook solution and the ANSYS solution is due to the different boundary conditions for each solution. For the ANSYS solution, one edge of the composite bar was completely fixed so that a static analysis could be performed. Also, the force was applied to only one end of the composite specimen. In the textbook solution, no edges were fixed, and a force was applied to the opposite ends of the composite specimen. The difference in the results is due to the different loading conditions for each solution. If a dynamic analysis using ANSYS had been performed, then the loading conditions for each solution could have remained identical. This would have improved the accuracy of the ANSYS results.

3.3 Types of Models Developed

Three ANSYS models were developed to show that a FEA program can be successfully utilized as a method of nondestructive evaluation for structural materials. A heat and a

stress model of a defected aluminum plate and a stress model involving a composite material were modeled.

An aluminum plate with a defect was chosen to show that ANSYS is capable of modeling a defect in an aluminum structure. This particular model could be applied to NASA's painted rocket motor structure. The rocket motor is painted with a thermal coating to prevent the motor from overheating. The ANSYS model is capable of modeling the effects a foreign object between the motor and the thermal coating has on the overall performance of the structure.

Because the use of composite materials in the aerospace industry has increased, a FEA involving a composite material was chosen. One particular concern with the use of composite materials is the effect a debond within the composite has on the overall performance of the composite material. Shearography is a type of NDE technique used to locate debonds in composite materials. With the use of a FEA program, the actual effects these debonds have on the overall performance of the composite structure can be evaluated. From this information, an engineer would then be able to determine whether or not a particular debond in a composite structure would result in a catastrophic failure of the structure.

3.3.1 Stress Analysis of an Aluminum Plate with a Defect

The aluminum plate with a defect was modeled to show the effects that a defect has on a stress analysis of an aluminum plate. For this model, the defect was modeled as a teflon pad on the top surface of the aluminum plate.

This particular model was modeled using the ANSYS stif 42 element which is a two-dimensional isoparametric solid. The aluminum plate had a total of 16 elements, while the teflon pad was modeled using four elements. Table 5 shows the material properties used in the ANSYS model.

Table 5. Material Properties Used in the ANSYS Model

Material	E_x (Pa)	ρ (kg/m^3)
Aluminum	7E10	2700
Teflon	500E6	2000

For this analysis, the edge of the aluminum plate was fixed while a pressure of 50 KPa was applied to the opposite edge. Figure 10 shows the schematic for this model.

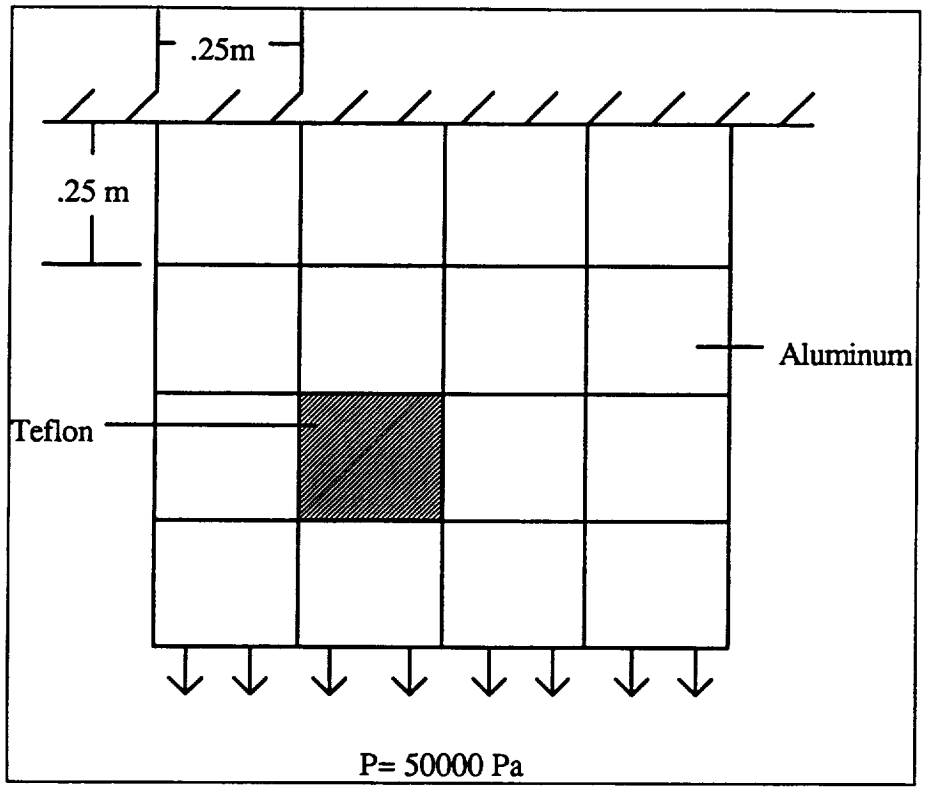

Figure 10. Schematic of Aluminum Plate with a Defect

3.2.2 Heat Transfer Analysis of an Aluminum Plate with a Defect

Similar to the stress analysis of the aluminum plate, a heat transfer analysis was also performed. This analysis was performed using the ANSYS stif 55 element which is a two-dimensional isoparametric thermal solid. Again, the defect was modeled as a teflon pad on the surface of the aluminum plate. The aluminum plate was modeled using 16 elements, and the teflon defect was modeled using 4 elements. Table 6 contains the material properties used in the ANSYS code.

Table 6. Material Properties Used in the Thermal ANSYS Model

Material	ρ (kg/m^3)	k (W/mK)	c (J/Kg K)
Aluminum	2700	237	903
Teflon	2200	.35	-----

For this analysis, three sides of the plate were held at a constant temperature of 500 K. The remaining edge was exposed to air at 300 K. Figure 11 shows the schematic for this model.

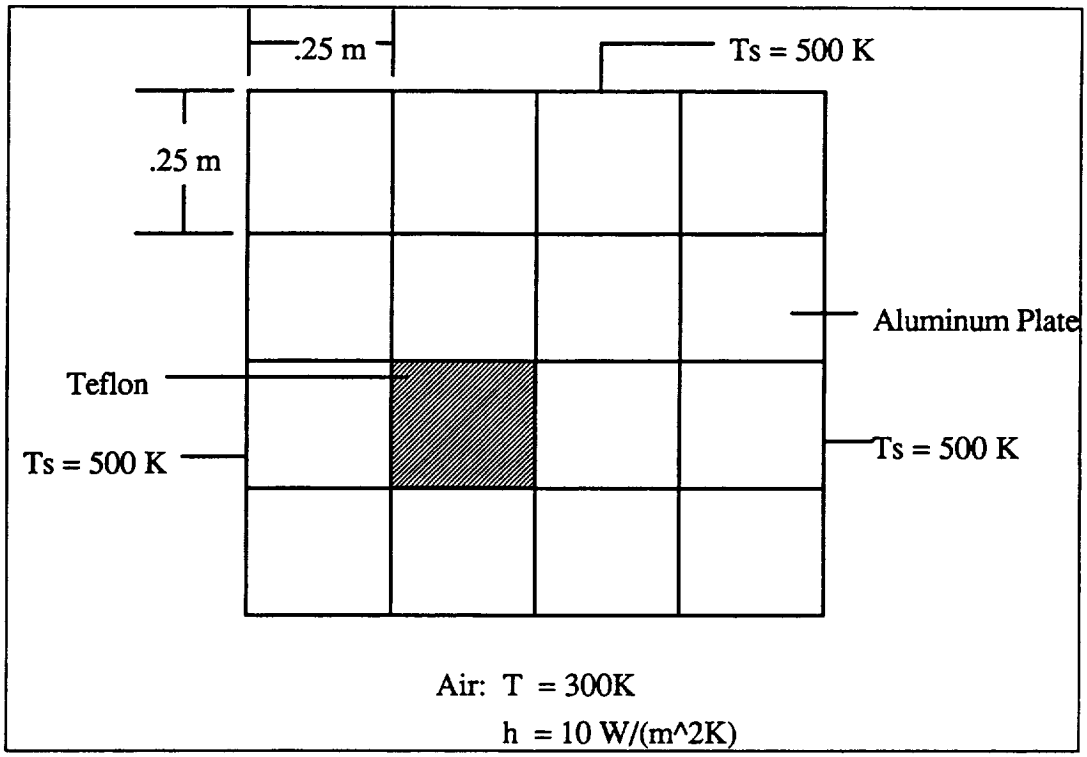

Figure 11. ANSYS Model for Thermal Analysis

3.3.3 Debond in Composite

A debonded composite material could not be modeled using the ANSYS composite element, stif 91. This element type assumes that all layers in the composite are perfectly bonded. Also, while this element allows different thicknesses for each ply within the composite, the overall dimensions of the composite plies is assumed to be equal. Therefore, the three-dimensional isoparametric solid element, stif 45, was chosen.

The composite modeled is a high modulus graphite epoxy composite with a stacking sequence of $[0,90]_S$. This particular composite was chosen because it was one of the very few composites with given material properties in the correct form for the ANSYS input code. Each ply was assumed a thickness of .004m; thus, the total thickness of the plate was .016m. Table 7 contains the material properties for the composite as well as the assumed material properties for the debond.

Table 7. Material Properties Used in the ANSYS Model

Material	$E_X=E_Y$(Pa)	G_{XY} (Pa)	ν_{XY}
Graphite Epoxy	92.46E9	4.5E9	.038
Debond	92.46E15	-----	-----

The entire ANSYS model consists of 4 layers of elements, one layer for each ply in the composite. To account for the fiber orientation, the element coordinate system for each layer of elements was rotated accordingly with respect to the global coordinate system.

The debond in the composite was modeled as elements within the composite plate with different material properties. Two debonds were placed within the composite plate. The first debond was placed in the second ply and the second debond was placed in the third ply as shown in figure 12.

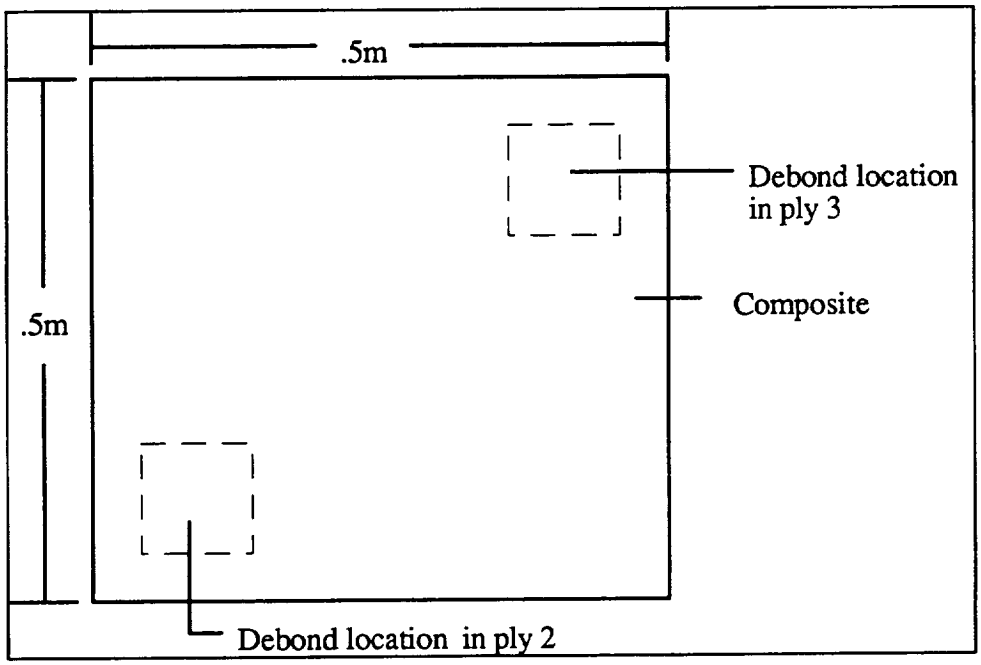

Figure 12. Position of Debonds in Composite Plate

To stress the plate, a pressure of 5000 Pa was applied to the bottom surface of the plate. The four corner nodes of layer 1 were completely fixed. Figure 13 shows the schematic for this model.

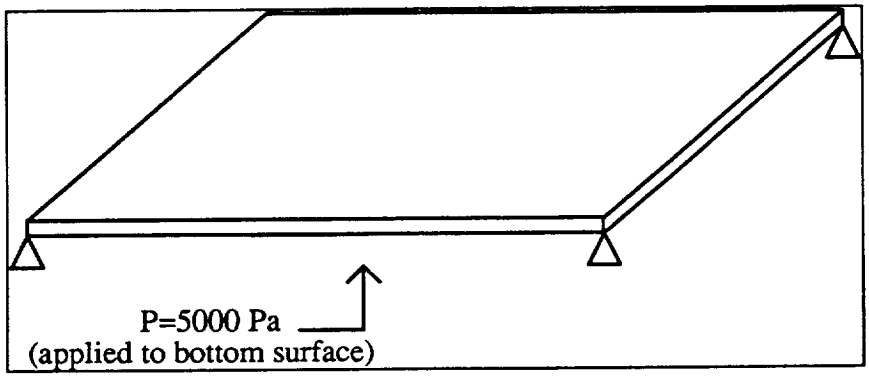

Figure 13. Schematic of Stressed Plate

4.0 RESULTS

4.1 Stress and Thermal Analysis of Aluminum Plate with Defect

It can be seen from the ANSYS stress plot in appendix 4 that the maximum stress occurs around the defect. This is due to the different modulus of elasticity of the teflon.

Similarly, it is evident in the ANSYS temperature distribution display in appendix 3, the exact location of the teflon. Again, this is due to the different material properties. Teflon has a much lower thermal conductivity that aluminum. This is seen in the slightly lower temperature distribution in the teflon. If a larger teflon pad had been modeled on the aluminum plate, the temperature gradient would probably have been greater.

4.2 Stress Analysis of Debonded Composite

From observing the ANSYS displacement plot of the debonded composite in appendix 5, it may not be evident that a defect exists in the composite. However, when this displacement plot is compared to the displacement plot of a similar model with no debond in appendix 6, a difference can be seen. The displacement gradient where the debonds exist is actually lower than the displacement gradient of the no debond composite. This is due to the much higher modulus of elasticity that was assumed for the debond.

Similarly, the debonds are also evident in the stress plots found in appendix 5. A much higher stress occurs around the debonds.

5.0 CONCLUSION

ANSYS is a finite element analysis (FEA) program used in a wide variety of engineering analyses. Among the many applications of ANSYS is its use for nondestructive evaluation of composite materials.

While a finite element model cannot detect defects in an already built structure, it can be used as a "pre-model" to perform a structural analysis. ANSYS is capable of evaluating the structure under many different loading conditions. This application enables the designer to change the original design as needed.

FEA can also be used to aid in properly interpreting the results from other types of NDE methods such as shearography. Shearography measures the out of plane displacement caused by a defect in a material when the material is stressed. The defect can be seen as a fringe pattern that the engineer can understand. The same defect can also be modeled using a FEA program. The defect can be seen in stress plots and displacement plots when the model is stressed. While the shearography technique can only detect the debond, the FEA program can detect both the debond and the stresses the debond causes on the material.

With the use of a FEA program, the actual effects a defect has on the overall performance of a structure can be determined. From this information, an engineer would then be capable of determining whether or not a particular defect would have a catastrophic effect the structure.

With the increasing demand for composite materials, understanding how these materials behave given certain conditions is very important. ANSYS is a powerful tool which can be utilized to model this behavior and give the composite user a better understanding of the composite characteristics.

6.0 REFERENCES

1. J. A. Leendertz , **J. Phys. E 3** (1970) 214

2. J. A. Leendertz and J. N. Butters, **J. Phys. E 6** (1973) 1107-1110

3. Y. Y. Hung, **Opt. Eng. 21** (1982) 391-395.

4. Y. Y. Hung, **Opt. Eng. 21** (1982) 391-395.

5. Y. Y. Hung, *Manual on Experimental Methods for Mechanical Testing of Composites*, SEM, 1989, Bethel, CT, pp. 81-96.

6. P. Boone, **Exp. Mech.** (1973) 295-302

7. R. K. Mohanty, C. Joenathan, and R. S. Sirohi, **App. Opt. 24** (1985) 3106-3109.

8. C. Joenathan, A. R. Ganesan, and R. S. Sirohi, **App. Opt. 25** (1986) 3781-3784.

9. R. K. Mohanty, C. Joenathan, and R. S. Sirohi, **App. Opt. 25** (1986) 1661-1664.

10. C. J. Tay, et. al. *Optics and Lasers in Engineering*, 1990 Elsevier Science Publishers, Northern Ireland, pp. 13-24.

11. M. Owner-Peersen, App. Opt. 30 (1991) 2730-2738

12. S. L. Tol, H. M. Shang, F. S. Chau, C.J. Tay, **Opt. and Laser Tech. 23** (1991) 25-30.

13. Lawrence H. Van Vlack, *Elements of materials Science and Engineering*, 1985 Addison-Wesley Publishing Co., pp. 612-613.

14. Bhagwan Agarwal and Lawrence Broutman, *Analysis and Performance of Fiber Composites*, 1990 John Wiley & Sons, New York, pp. 166-170, pp.221-228.

15. Frank Incropera and David De Witt, *Introduction to Heat Transfer*, 1985 John Wiley & Sons, New York, pp. 152-155, pp.680-689.

16. ASTM International, *Volume 1 Engineered Materials Handbook: Composites*, 1987, p.223.

7.0 APPENDICES

Examples of ANSYS code and results from those finitel element analyses.

Appendix 1. Comparison with heat transfer example.

Appendix 2. Comparison of performance of fiber reinforced composite material.

Appendix 3. Thermal analysis of aluminum plate with debond (teflon pad).

Appendix 4. Static stress analysis of aluminum plate with debond (teflon pad).

Appendix 5. Analysis of composite with debond.

Appendix 6. Analysis of composite with no debond.

Appendix 7. Equations used to transform elastic constants for ANSYS input code.

Appendix 8. Symbols used in this report.

Appendix 1. Comparison with heat transfer example

```
/PREP7
! ********************************************************************
! INTRODUCTION TO HEAT TRANSFER BY INCROPERA & DE WITT
! EXAMPLE 4.3 PAGE 152-155
! ********************************************************************

KAN,-1
ET,1,55
MP,KXX,1,1 $MP,DENS,1,2645 $MP,C,1,960
KTEMP,-1
K,1,0 $K,2,1,0 $K,3,1,1 $K,4,0,1
L,1,2 $L,2,3 $L,3,4 $L,4,1
A,1,2,3,4 $ELSIZ,.25,,2 $AMESH,1
NSEL,NODE,1,10 $NASEL,NODE,14,16
NT,ALL,TEMP,500
LCVS,3,10,300
ITER,-10,10
NALL $EALL
AFWR $FINI
/INPUT,27
FINI
```

```
 PRINT NODAL TEMPERATURES

          ***** POST1 NODAL TEMPERATURE LISTING *****

LOAD STEP     1  ITERATION=    10  SECTION=  1
TIME=   0.00000          LOAD CASE=  1

NODE      TEMP
1    500.00000
2    500.00000
3    500.00000
4    500.00000
5    500.00000
6    500.00000
7    500.00000
8    500.00000
9    500.00000
10   500.00000
11   350.59795
12   339.68809
13   350.59795
14   500.00000
   ****** POST1 NODAL TEMPERATURE LISTING *****

LOAD STEP     1  ITERATION=    10  SECTION=  1
TIME=   0.00000          LOAD CASE=  1

    NODE      TEMP
15    500.00000
16    500.00000
17    491.15093
18    487.48116
19    491.15093
20    475.82119
21    465.90506
22    475.82119
23    443.78274
24    418.24961
25    443.78274

MAXIMUMS
NODE          1
VALUE     500.00000


 ***** ROUTINE COMPLETED *****  CP =         1.386

SYSTEM= BCS-SEATTLE/CRAY   REVISION= 4.4      A 16
FOR SUPPORT CALL GLENN REILING     PHONE (205) 971-7426     TWX
CURRENT JOBNAME=file

/EOF ENCOUNTERED ON FILE 5


PREP7 AFWRITE OR SFWRITE WARNING MESSAGES =    0
NUMBER OF SOLUTION PHASE WARNING MESSAGES =    0

DATA INPUT WRITTEN ON FILE18
```

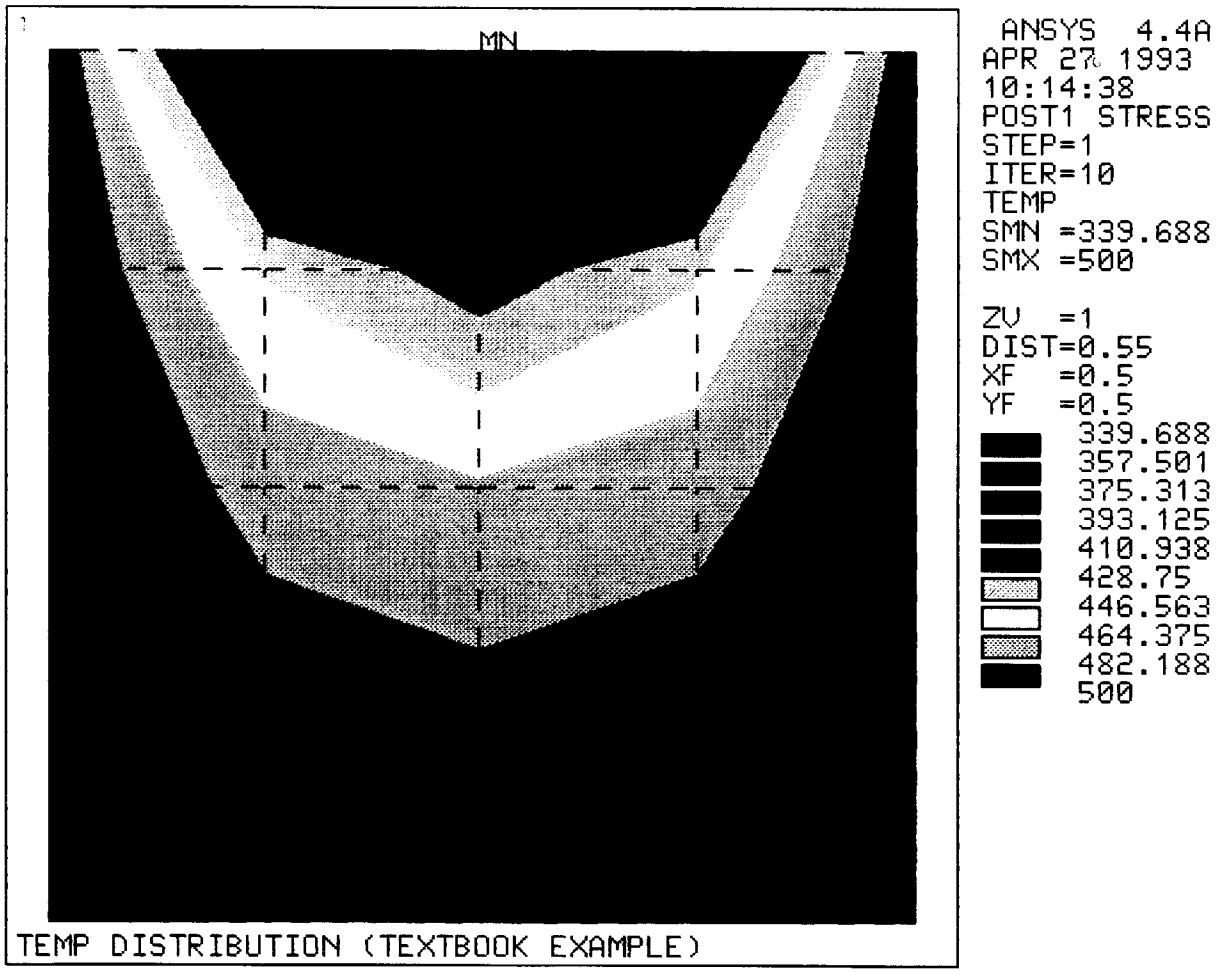


```
PLNS,TEMP

 PRODUCE STRESS PLOT,  LABEL= TEMP  KAVG= 0
 POST1 -INP=
```

Figure 14. Temperature Distribution for Heat Transfer Problem

Appendix 2. Comparison of performance of fiber reinforced composite material

```
/PREP7
ET,1,91,,,8,,,1
! ********************************************************************
!                  THIS IS EXAMPLE 6.9 PAGES 223-228
!      SOURCE:  ANALYSIS AND PERFORMANCE OF FIBER REINFORCED COMPOSITES
!          BY:  AGARWAL & BROUTMAN
!
! GIVEN MATERIAL PROPERTIES:        EL = 40E9 Pa     GLT = 4E9 Pa
! ********************************************************************
! STACKING SEQUENCE:                [0,+45,-45,90]s
! DIMENSIONS:                       250x200x2 mm
! PLY THICKNESS:                    25E-5 m
! ********************************************************************
! TRANSFORMED MATERIAL PROPERTIES
!  ANGLE        EX(GPa)          EY(GPa)          GXY(GPa)         VXY
!    0          40               10               4                .285
!  +45          11.09            11.08            7.18             .386
!  -45          11.09            11.08            7.18             .386
!   90          10               40               4                .0713
! ********************************************************************
R,1,1,0,25E-5 $RMORE,2,45,25E-5 $RMORE,2,-45,25E-5 $RMORE,3,90,25E-5
RMORE,1,0,25E-5 $RMORE,2,45,25E-5 $RMORE,2,-45,25E-5 $RMORE,3,90,25E-5
MP,EX,1,40E9 $MP,EY,1,10E9 $MP,GXY,1,4E9 $MP,PRXY,1,.285
MP,EX,2,11.09E9 $MP,EY,2,11.08E9 $MP,GXY,2,7.18E9 $MP,PRXY,2,.386
MP,EX,3,10E9 $MP,EY,3,40E9 $MP,GXY,3,4E9 $MP,PRXY,3,.0713

K,1 $K,2,.25 $K,3,.25,.02 $K,4,0,.02
L,1,2 $L,2,3 $L,3,4 $L,4,1
A,1,2,3,4
LDVS,1,.025 $LDVS,3,.025 $LDVS,2,1 $LDVS,4,1
AMESH,1

KD,1,ALL,0 $KD,4,ALL,0
D,1,ALL $D,44,ALL $D,24,ALL
D,ALL,UY,0 $D,ALL,UZ,0 $D,ALL,ROTX,0
F,2,FX,0 $F,22,FX,0 $F,23,FX,0
KPALL $NALL $LWRI

KD,1,ALL,0 $KD,4,ALL,0
D,1,ALL $D,44,ALL $D,24,ALL
D,ALL,UY,0 $D,ALL,UZ,0 $D,ALL,ROTX,0
F,2,FX,2000 $F,22,FX,2000 $F,23,FX,2000
KPALL $NALL $LWRI

KD,1,ALL,0 $KD,4,ALL,0
D,1,ALL $D,44,ALL $D,24,ALL
D,ALL,UY,0 $D,ALL,UZ,0 $D,ALL,ROTX,0
F,2,FX,4000 $F,22,FX,4000 $F,23,FX,4000
KPALL $NALL $LWRI

KD,1,ALL,0 $KD,4,ALL,0
D,1,ALL $D,44,ALL $D,24,ALL
D,ALL,UY,0 $D,ALL,UZ,0 $D,ALL,ROTX,0
F,2,FX,6000 $F,22,FX,6000 $F,23,FX,6000
KPALL $NALL $LWRI

KD,1,ALL,0 $KD,4,ALL,0
D,1,ALL $D,44,ALL $D,24,ALL
D,ALL,UY,0 $D,ALL,UZ,0 $D,ALL,ROTX,0
F,2,FX,8000 $F,22,FX,8000 $F,23,FX,8000
```

```
KPALL $NALL $LWRI

KD,1,ALL,0 $KD,4,ALL,0
D,1,ALL $D,44,ALL $D,24,ALL
D,ALL,UY,0 $D,ALL,UZ,0 $D,ALL,ROTX,0
F,2,FX,10000 $F,22,FX,10000 $F,23,FX,10000
KPALL $NALL $LWRI

KD,1,ALL,0 $KD,4,ALL,0
D,1,ALL $D,44,ALL $D,24,ALL
D,ALL,UY,0 $D,ALL,UZ,0 $D,ALL,ROTX,0
F,2,FX,12000 $F,22,FX,12000 $F,23,FX,12000
KPALL $NALL $LWRI

AFWR $FINI
/INPUT,27 $FINI
```

```
 LOAD STEP      1  ITERATION=      1  SECTION=  1
 TIME=    0.00000          LOAD CASE=   1

   NODE       UX                UY                UZ
MAXIMUMS
NODE            0                 0                 0
VALUE     0.00000000        0.00000000        0.00000000

 LOAD STEP      2  ITERATION=      1  SECTION=  1
 TIME=    0.00000          LOAD CASE=   1

   NODE       UX                UY                UZ
MAXIMUMS
NODE            2                 0                 0
VALUE     0.14016140E-02    0.00000000        0.00000000

 LOAD STEP      3  ITERATION=      1  SECTION=  1
 TIME=    0.00000          LOAD CASE=   1

   NODE       UX                UY                UZ
MAXIMUMS
NODE            2                 0                 0
VALUE     0.28032281E-02    0.00000000        0.00000000

 LOAD STEP      4  ITERATION=      1  SECTION=  1
 TIME=    0.00000          LOAD CASE=   1

   NODE       UX                UY                UZ
MAXIMUMS
NODE            2                 0                 0
VALUE     0.42048421E-02    0.00000000        0.00000000

 LOAD STEP      5  ITERATION=      1  SECTION=  1
 TIME=    0.00000          LOAD CASE=   1

   NODE       UX                UY                UZ
MAXIMUMS
NODE            2                 0                 0
VALUE     0.56064562E-02    0.00000000        0.00000000


 LOAD STEP      6  ITERATION=      1  SECTION=  1
 TIME=    0.00000          LOAD CASE=   1

   NODE       UX                UY                UZ

MAXIMUMS
NODE            2                 0                 0
VALUE     0.70080702E-02    0.00000000        0.00000000


 LOAD STEP      7  ITERATION=      1  SECTION=  1
 TIME=    0.00000          LOAD CASE=   1

   NODE       UX                UY                UZ
MAXIMUMS
NODE            2                 0                 0
VALUE     0.84096842E-02    0.00000000        0.00000000
```

Appendix 3. Thermal analysis of Al plate with debond

```
/PREP7
! ********************************************************************
! ALUMINUM PLATE WITH TEFLON PAD (2-D ANALYSIS)
!
! ASSUMED:      DIMENSIONS OF PLATE: 1m x 1m
!               THREE SIDES OF THE PLATE ARE KEPT AT 500 K
!               REMAINING SURFACE IS EXPOSED TO AIR AT 300 K
!               h = 10 W/(m^2 K)
! ********************************************************************
! MATERIAL PROPERTIES
! REFERENCE:    INTRODUCTION TO HEAT TRANSFER BY INCROPERA & DE WITT
!               PAGES 669 & 679
! ALUMINUM:     DENSITY = 2700 kg/m^3
!               k = 237 W/(m K)
!               c = 903 J/(kg K)
! TEFLON:       DENSITY = 2200 kg/m^3
!               k = .35 W/(m K)
! ********************************************************************
KAN,-1
KTEMP,-1
ET,1,55
MP,DENS,1,2700 $MP,KXX,1,237 $MP,C,1,903
MP,DENS,2,2200 $MP,KXX,2,.35

MAT,1
K,1 $K,2,1 $K,3,1,1 $K,4,0,1
L,1,2 $L,2,3 $L,3,4 $L,4,1 $A,1,2,3,4
LDVS,1,.25 $LDVS,2,.25 $LDVS,3,.25 $LDVS,4,.25
AMESH,1

MAT,2
K,5,.25,.25 $K,6,.5,.25 $K,7,.5,.5 $K,8,.25,.5
L,5,6 $L,6,7 $L,7,8 $L,8,5 $A,5,6,7,8
LDVS,5,.2 $LDVS,6,.2 $LDVS,7,.2 $LDVS,8,.2
AMESH,2

NUMMRG,ALL
NSEL,NODE,6,16 $NT,ALL,TEMP,500
LCVS,1,10,300 $LCVS,3,10,300
NALL $KPALL $EALL
AFWR $FINI
/INPUT,27 $FINI
```

PRINT NODAL TEMPERATURES

***** POST1 NODAL TEMPERATURE LISTING *****

LOAD STEP 1 ITERATION= 1 SECTION= 1
TIME= 0.00000 LOAD CASE= 1

NODE	TEMP
1	496.70333
2	496.70326
3	496.59583
4	496.19139
5	496.59579
6	500.00000
7	500.00000
8	500.00000
9	500.00000
10	500.00000
11	500.00000
12	500.00000
13	500.00000
14	500.00000
15	500.00000
16	500.00000
17	498.22114
18	497.93620
19	498.22101
20	499.32109
21	499.02014
22	499.32132
23	499.74826
24	499.64489
25	499.74829
28	498.48815
30	498.58802
32	498.76113
33	498.66126
34	498.62464

MAXIMUMS

NODE	6
VALUE	500.00000

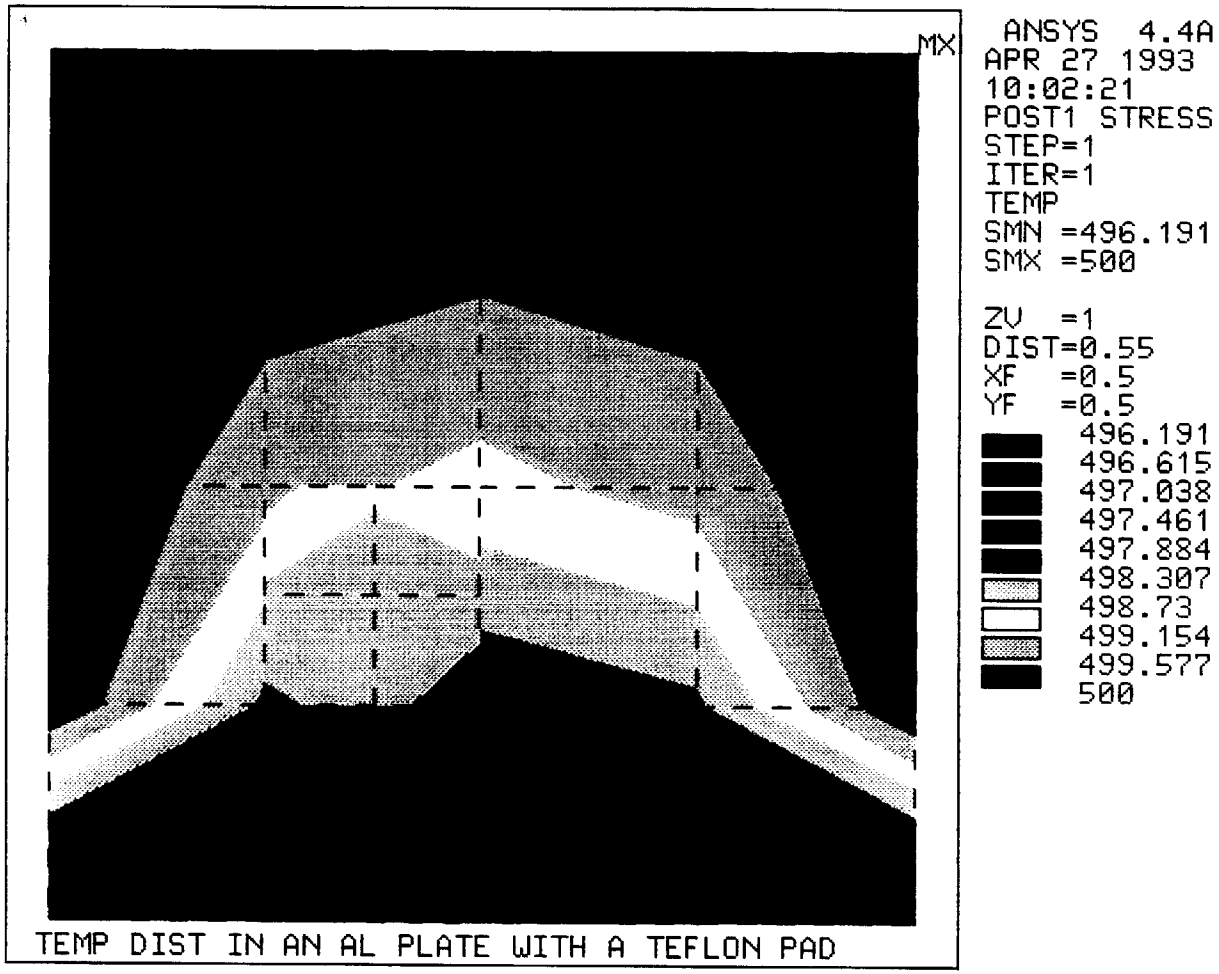


```
PLNS,TEMP

 PRODUCE STRESS PLOT,  LABEL= TEMP  KAVG= 0
 POST1 -INP=
```

Figure 15. Temperature Distribution for Al Plate with Debond (Teflon Pad)

Appendix 4. Static stress analysis of Al plate with debond (teflon pad)

```
/PREP7
! *********************************************************************
! ALUMINUM PLATE WITH TEFLON PAD (2-D ANALYSIS)
! DIMENSIONS:  1m x 1m
! MATERIAL PROPERTIES
! ELEMENTS OF MATERIALS SCIENCE AND ENGINEERING BY VAN VLACK (P.612 & 613)
!       ALUMINUM:       EX = 7E10 Pa
!                       DENSITY = .0027 g/m^3
!       TEFLON:         EX = 500E6 Pa
!                       DENSITY = .002 g/m^3
! *********************************************************************

ET,1,42
MP,EX,1,7E10 $MP,DENS,1,.0027
MP,EX,2,500E6 $MP,DENS,2,.002
MAT,1
K,1 $K,2,1 $K,3,1,1 $K,4,0,1
L,1,2 $L,2,3 $L,3,4 $L,4,1 $A,1,2,3,4
LDVS,1,.25 $LDVS,2,.25 $LDVS,3,.25 $LDVS,4,.25
AMESH,1

MAT,2
K,5,.25,.25 $K,6,.5,.25 $K,7,.5,.5 $K,8,.25,.5
L,5,6 $L,6,7 $L,7,8 $L,8,5 $A,5,6,7,8
LDVS,5,.5 $LDVS,6,.5 $LDVS,7,.5 $LDVS,8,.5
AMESH,2

NUMMRG,ALL
NSEL,NODE,1,5 D,ALL,ALL,0 $LPSF,3,50000
KPALL $NALL
```

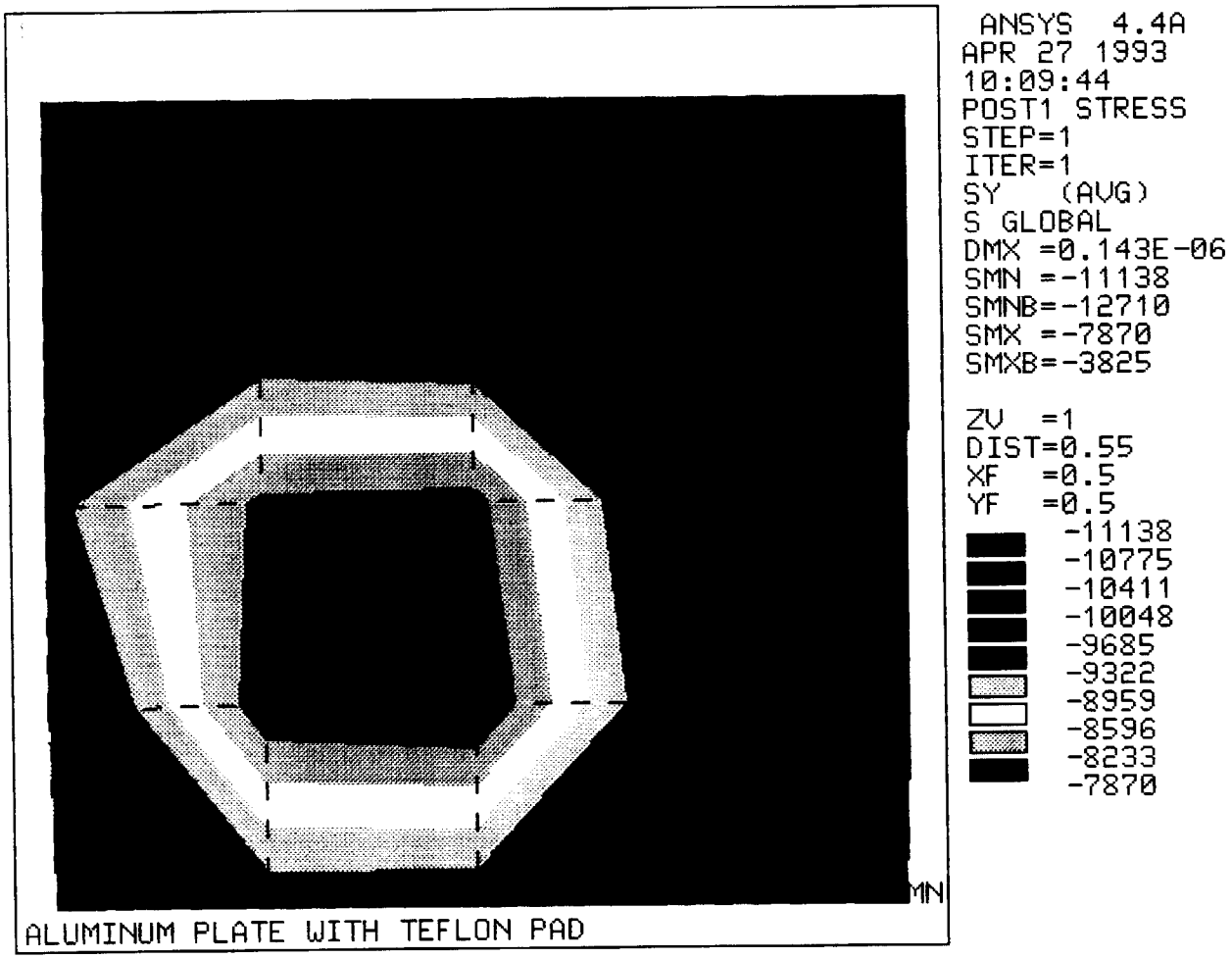


```
PLNS,SY

 PRODUCE STRESS PLOT,  LABEL= SY     KAVG= 0
 POST1 -INP=
```

Figure 16. Stress plot SY of Al plate with teflon plate

Appendix 5. Analysis of composite with debond

```
/PREP7
! *********************************************************************
! MATERIAL PROPERTIES FOR HIGH MODULUS GRAPHITE EPOXY
! REFERENCE:  VOLUME 1:  ENGINEERED MATERIALS HANDBOOK- COMPOSITES (P.223)
!             STACKING SEQUENCE [0/90]s
!             PLY THICKNESS = .004m
!             DIMENSIONS OF PLATE:  .5m x .5m x ..016m
              EX = EY = 92.46Pa
!             GXY = 4.5 GPa
!             PRXY = .038
! *********************************************************************
! MATERIAL PROPERTIES FOR DEBOND (ASSUMED)
!              EX = EY = 92.46E15
! *********************************************************************

ET,1,45
MP,EX,1,92.46E9 $MP,GXY,1,4.5E9 $MP,prXY,1,.038
MP,EX,2,92.46E15

! LAYER 1
K,1 $K,2,.5 $K,3,.5,.004 $K,4,0,.004 $K,5,0,0,.5
L,1,2 $L,2,3 $L,3,4 $L,4,1 $L,5,1
A,1,2,3,4 $VDRAG,1,,,,,,5 $ELSIZE,.08,,2
LOCAL,11,0,0,0,0,,,0
MAT,1 $ESYS,11 $VMESH,1

! LAYER 2
CSYS,0
K,10,0,.004 $K,11,.5,.004 $K,12,.5,.008 $K,13,0,.008
K,14,0,.004,.5
L,10,11 $L,11,12 $L,12,13 $L,13,10 $L,14,10
A,10,11,12,13 $VDRAG,7,,,,,,18 $ELSIZE,.08,,2
LOCAL,12,0,0,0,0,,,90
MAT,1 $ESYS,12 $VMESH,2

MAT,2
E,109,103,231,237,110,104,232,238
E,103,97,225,231,104,98,226,232
E,108,102,230,236,109,103,231,237
E,102,96,224,230,103,97,225,231

! LAYER 3
CSYS,0
K,19,,.008 $K,20,.5,.008 $K,21,.5,.012 $K,22,0,.012
K,23,0,.008,.5
L,19,20 $L,20,21 $L,21,22 $L,22,19 $L,23,19
A,19,20,21,22 $VDRAG,13,,,,,,31 $ELSIZE,.08,,2
LOCAL,13,0,0,0,0,,,90
MAT,1 $ESYS,13 $VMESH,3

MAT,2
E,251,245,373,379,252,246,374,380
E,252,246,374,380,253,247,375,381
E,245,239,367,373,246,240,368,374
E,246,240,368,374,247,241,369,375
```

```
! LAYER 4
CSYS,0
K,28,,.012 $K,29,.5,.012 $K,30,.5,.016 $K,31,0,.016
K,32,0,.012,.5
L,28,29 $L,29,30 $L,30,31 $L,31,28 $L,32,28
A,28,29,30,31 $VDRAG,19,,,,,,32 $ELSIZE,.08,,2
MAT,1 $VMESH,4

NUMMRG,ALL
NSEL,NODE,1,2 $NASEL,NODE,17,17 $NASEL,NODE,24,24
D,ALL,ALL,0
APSF,2,5000
NALL,KPALL,EALL
WAVES
AFWR $FINI
/INPUT,27 $FINI
```

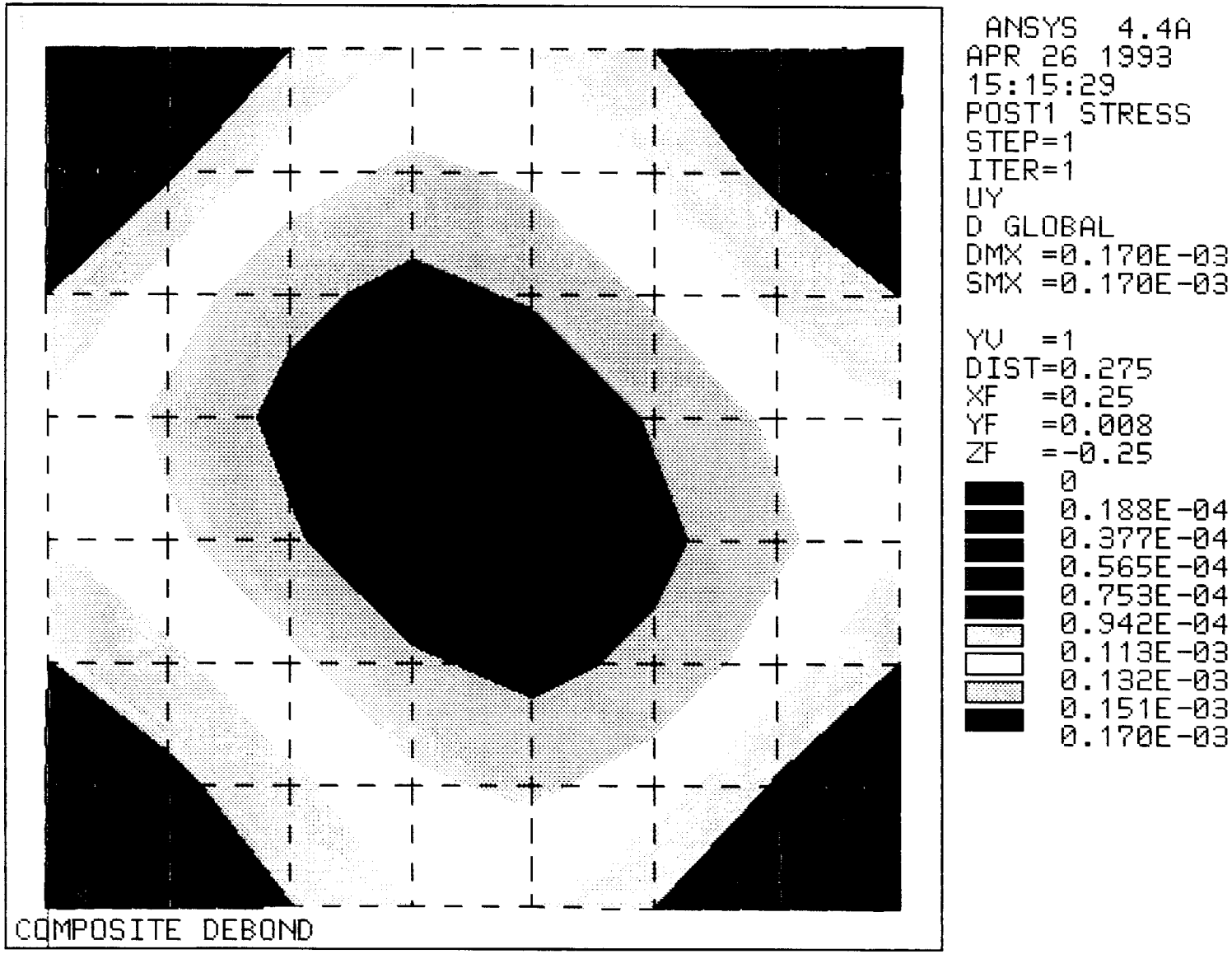


```
PRODUCE STRESS PLOT,  LABEL= UY     KAVG= 0

*** NOTE - DEFAULT DEVICE 4207      WILL BE USED.
POST1 -INP=
```

Figure 17. Y-Displacement Plot for Debonded Composite

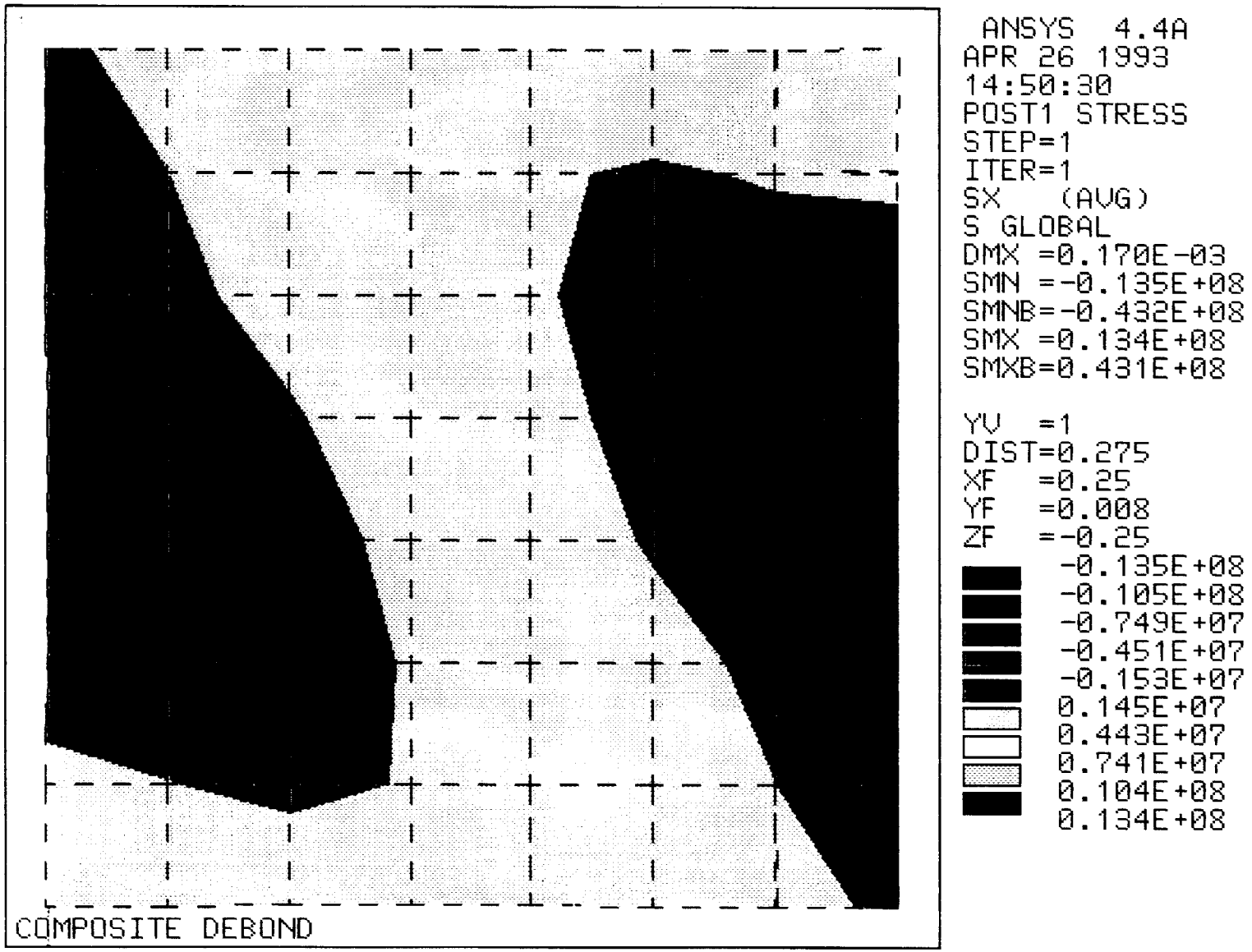


```
PRODUCE STRESS PLOT,  LABEL= SX     KAVG= 0

*** NOTE - DEFAULT DEVICE 4207      WILL BE USED.
POST1 -INP=
```

Figure 18. Stress plot (SX) of debonded composite (Top layer of 4 Plies)

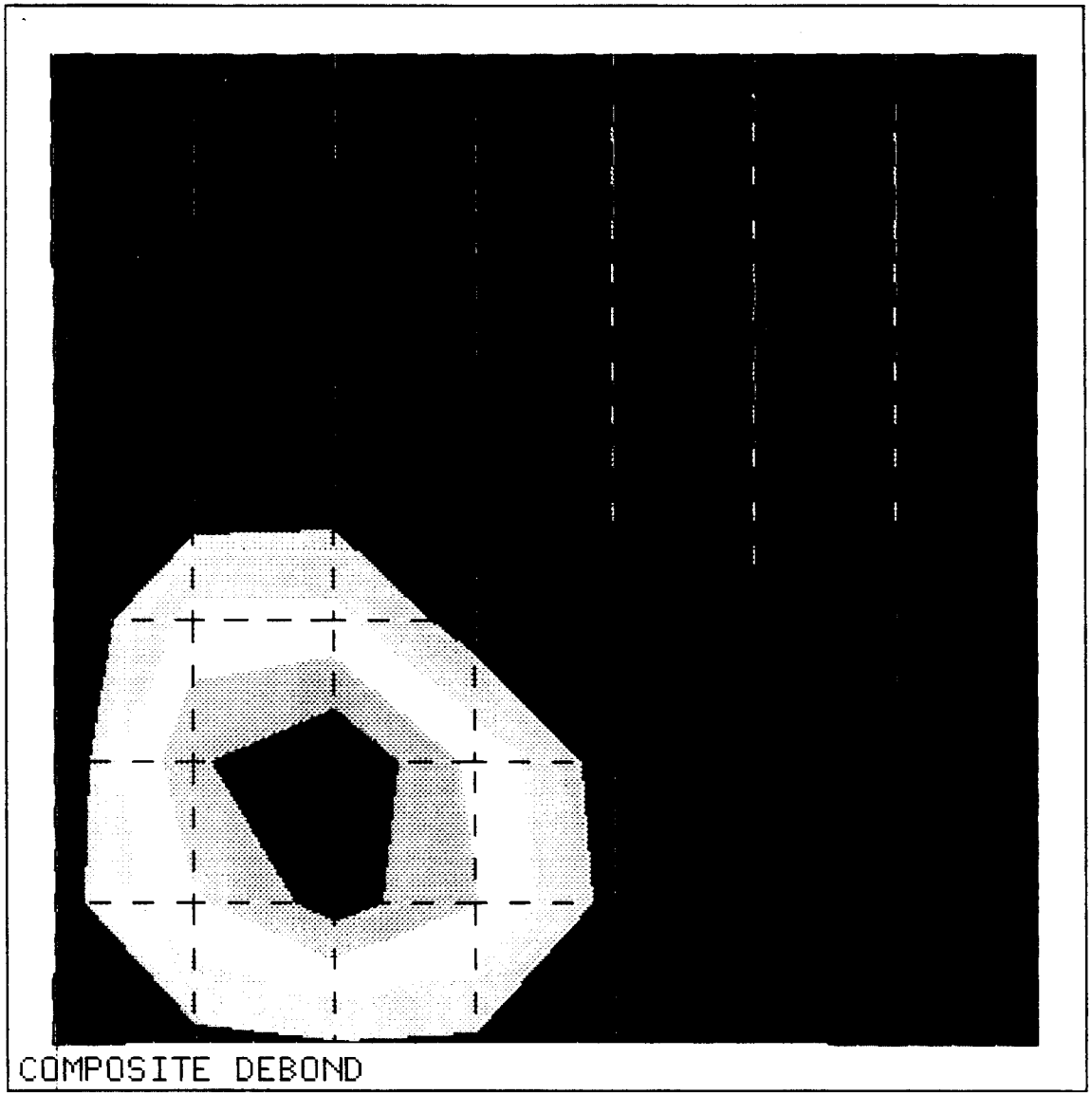


```
***WARNING ***                                  CP=      11.642   TIME=   15.03139
THE SELECTED ELEMENT SET CONTAINS MIXED MATERIALS--
    THIS COULD INVALIDATE ERROR ESTIMATION
POST1 -INP=
```

Figure 19. Stress plot (SX) of debonded composite (Second layer of 4 Plies)

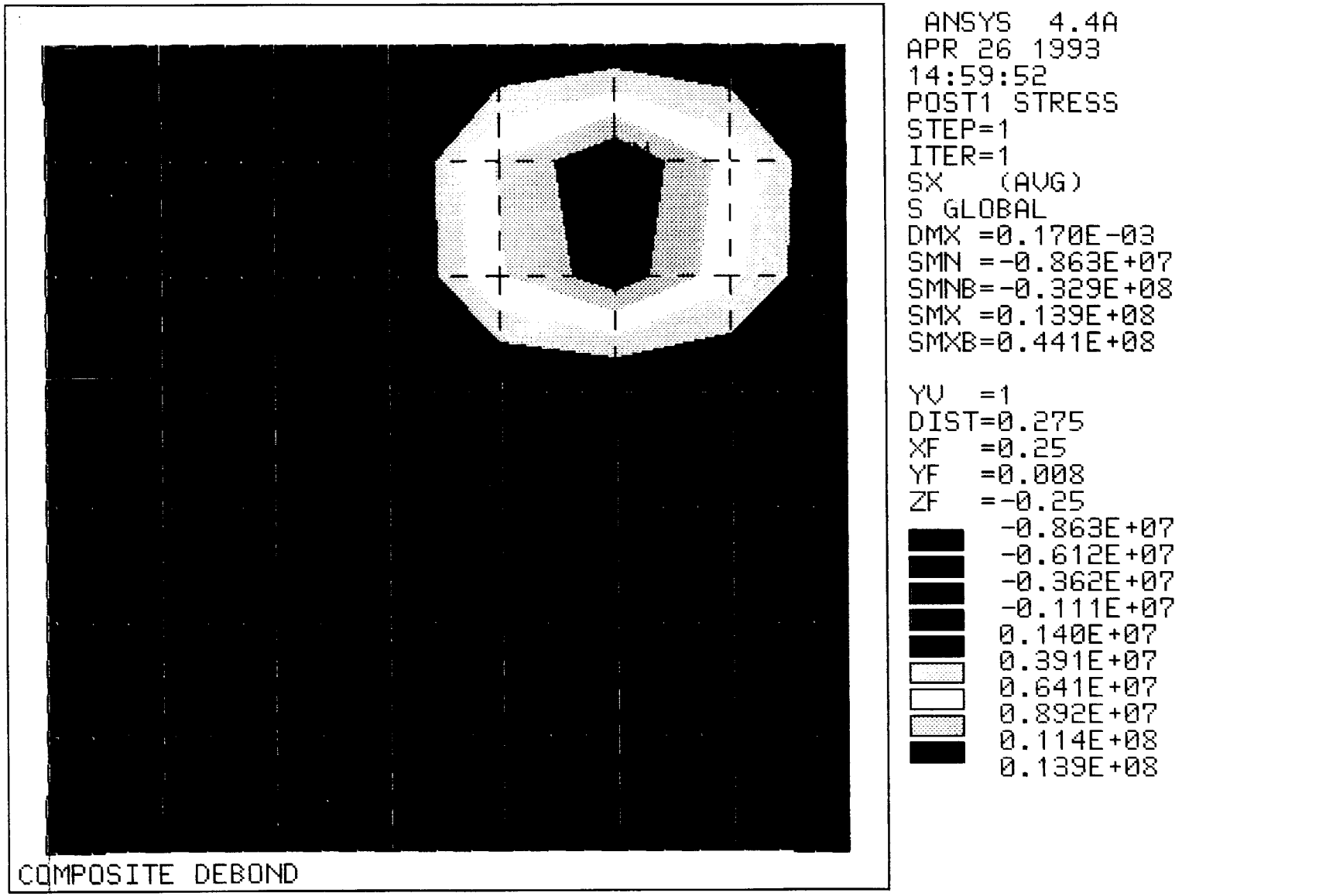


```
***WARNING ***                                  CP=      10.878   TIME=   14.99778
THE SELECTED ELEMENT SET CONTAINS MIXED MATERIALS--
    THIS COULD INVALIDATE ERROR ESTIMATION
POST1 -INP=
```

Figure 20. Stress plot (SX) of debonded composite (Third layer of 4 Plies)

Appendix 6. Analysis of composite with no debond

```
/PREP7
! ********************************************************************
! COMPOSITE WITH NO DEBOND
! ********************************************************************
! MATERIAL PROPERTIES FOR HIGH MODULUS GRAPHITE EPOXY
! REFERENCE:  VOLUME 1:  ENGINEERED MATERIALS HANDBOOK- COMPOSITES (P.223)
!             STACKING SEQUENCE [0/90]s
!             PLY THICKNESS = .004m
!             DIMENSIONS OF PLATE:  .5m x .5m x ..016m
!             EX = EY = 92.46Pa
!             GXY = 4.5 GPa
!             PRXY = .038
! ********************************************************************

ET,1,45
MP,EX,1,92.46E9 $MP,GXY,1,4.5E9 $MP,prXY,1,.038
MP,EX,2,92.46E15

! LAYER 1
K,1 $K,2,.5 $K,3,.5,.004 $K,4,0,.004 $K,5,0,0,.5
L,1,2 $L,2,3 $L,3,4 $L,4,1 $L,5,1
A,1,2,3,4 $VDRAG,1,,,,,,5 $ELSIZE,.08,,2
LOCAL,11,0,0,0,0,,,0
MAT,1 $ESYS,11 $VMESH,1

! LAYER 2
CSYS,0
K,10,0,.004 $K,11,.5,.004 $K,12,.5,.008 $K,13,0,.008
K,14,0,.004,.5
L,10,11 $L,11,12 $L,12,13 $L,13,10 $L,14,10
A,10,11,12,13 $VDRAG,7,,,,,,18 $ELSIZE,.08,,2
LOCAL,12,0,0,0,0,,,90
MAT,1 $ESYS,12 $VMESH,2

! LAYER 3
CSYS,0
K,19,,.008 $K,20,.5,.008 $K,21,.5,.012 $K,22,0,.012
K,23,0,.008,.5
L,19,20 $L,20,21 $L,21,22 $L,22,19 $L,23,19
A,19,20,21,22 $VDRAG,13,,,,,,31 $ELSIZE,.08,,2
LOCAL,13,0,0,0,0,,,90
MAT,1 $ESYS,13 $VMESH,3

! LAYER 4
CSYS,0
K,28,,.012 $K,29,.5,.012 $K,30,.5,.016 $K,31,0,.016
K,32,0,.012,.5
L,28,29 $L,29,30 $L,30,31 $L,31,28 $L,32,28
A,28,29,30,31 $VDRAG,19,,,,,,32 $ELSIZE,.08,,2
MAT,1 $VMESH,4

NUMMRG,ALL
NSEL,NODE,1,2 $NASEL,NODE,17,17 $NASEL,NODE,24,24
D,ALL,ALL,0
APSF,2,5000
NALL,KPALL,EALL
WAVES
AFWR $FINI
/INPUT,27 $FINI
```

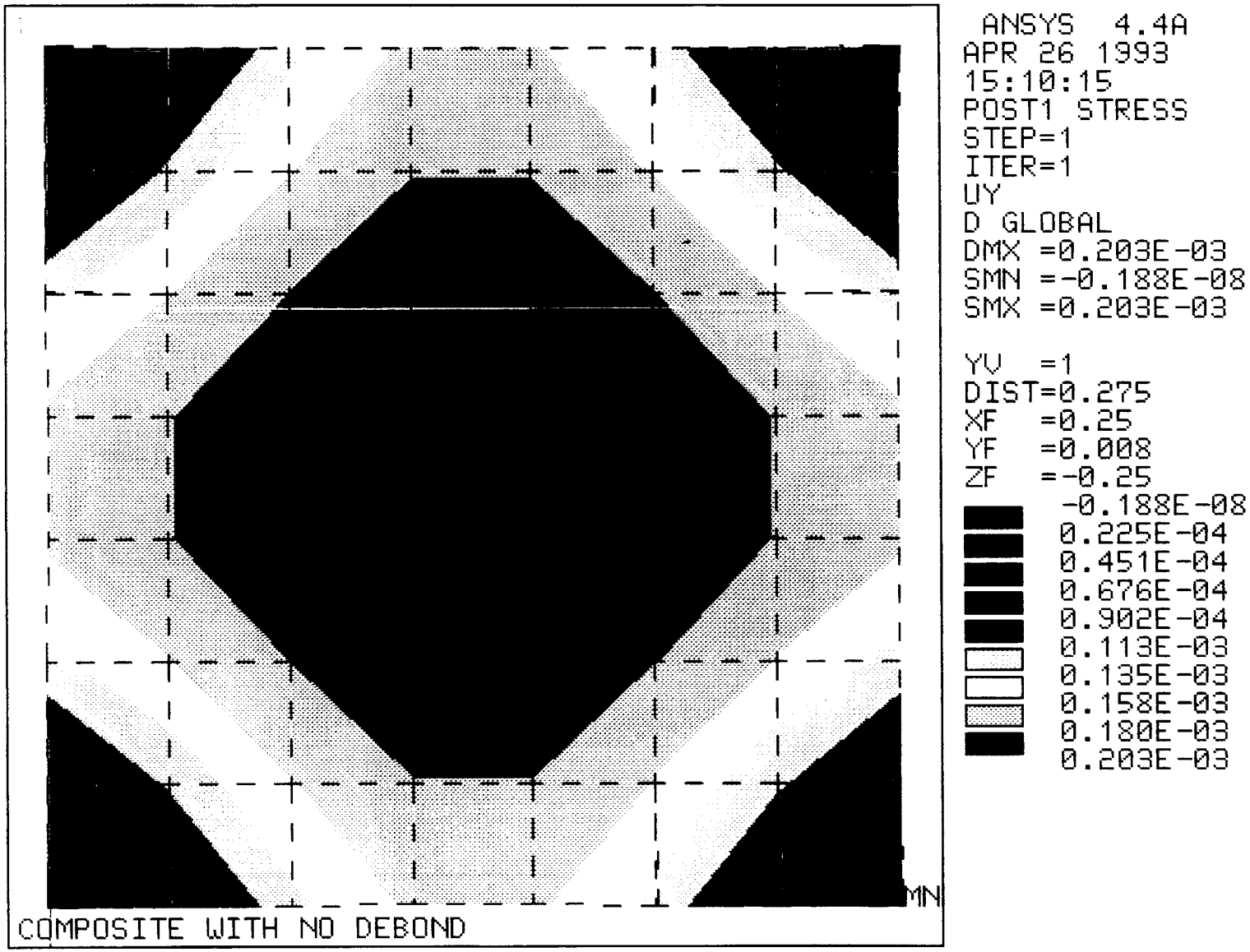


```
PLNS,UY

 PRODUCE STRESS PLOT,  LABEL= UY     KAVG= 0
 POST1 -INP=
```

Figure 21. Displacement plot in Y direction of composite with no debonds

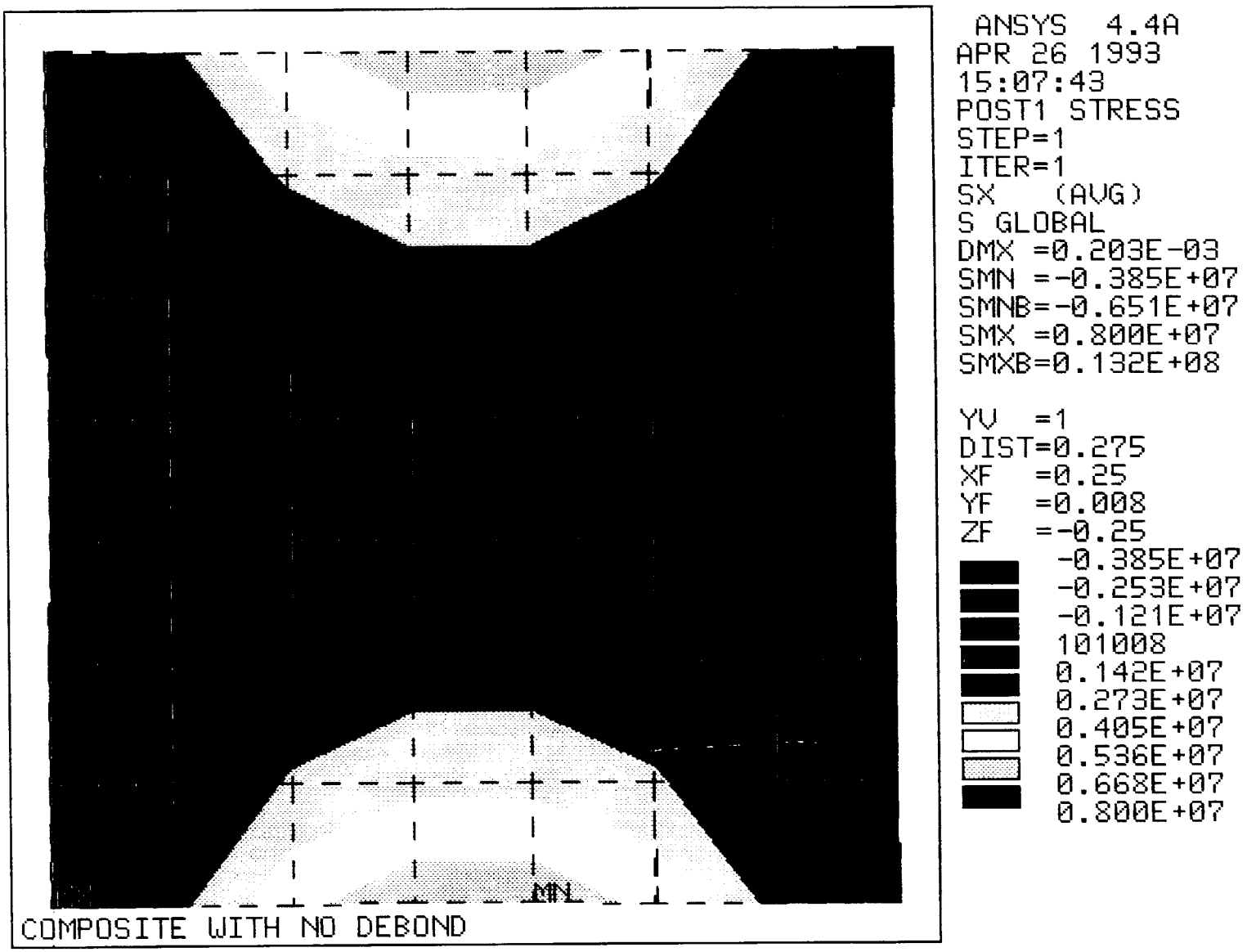

PRODUCE STRESS PLOT, LABEL= SX KAVG= 0

*** NOTE - DEFAULT DEVICE 4207 WILL BE USED.
POST1 -INP=

Figure 22. SX plots of Composite with no debonds.

Appendix 7. Equations used to transform elastic constants for ANSYS analysis

(Reference 14 pages 167-170)

$$\frac{1}{E_X} = \frac{\cos^4\Theta}{E_L} + \frac{\sin^4\Theta}{E_T} + \frac{1}{4}\left[\frac{1}{G_{LT}} - \frac{2\nu_{LT}}{E_L}\right]\sin^2 2\Theta$$

$$\frac{1}{E_Y} = \frac{\sin^4\Theta}{E_L} + \frac{\cos^4\Theta}{E_T} + \frac{1}{4}\left[\frac{1}{G_{LT}} - \frac{2\nu_{LT}}{E_L}\right]\sin^2 2\Theta$$

$$\frac{\nu_{XY}}{E_X} = \frac{\nu_{LT}}{E_L} - \frac{1}{4}\left[\frac{1}{E_L} + \frac{2\nu_{LT}}{E_L} + \frac{1}{E_T} - \frac{1}{G_{LT}}\right]\sin^2 2\Theta$$

$$\frac{\nu_{YX}}{E_Y} = \frac{\nu_{TL}}{E_T} - \frac{1}{4}\left[\frac{1}{E_L} + \frac{2\nu_{LT}}{E_L} + \frac{1}{E_T} - \frac{1}{G_{LT}}\right]\sin^2 2\Theta$$

$$\frac{1}{G_{XY}} = \frac{1}{E_L} + \frac{2\nu_{LT}}{E_L} + \frac{1}{E_T} - \left[\frac{1}{E_L} + \frac{2\nu_{LT}}{E_L} + \frac{1}{E_T} - \frac{1}{G_{LT}}\right]\cos^2 2\Theta$$

Appendix 8. Symbols used in this report

- $c(J/kg^{o}K)$ Specific Heat
- $E_L(Pa)$: Elastic Modulus in the Longitudinal Direction
- $E_T(Pa)$: Elastic Modulus in the Transverse Direction
- $E_x(Pa)$: Elastic Modulus in the x Direction
- $E_y(Pa)$: Elastic Modulus in the y Direction
- F(N): Force
- $G_{LT}(Pa)$: Shear Modulus in the LT direction
- $G_{xy}(Pa)$: Shear Modulus in the xy Direction
- $h(W/m^{2o}K)$: Convection Heat Transfer Coefficient
- $k(W/m^{o}K)$: Thermal Conductivity
- ν_{LT} (dimensionless): Poisson's Ratio in LT Direction
- ν_{xy} (dimensionless): Poisson's Ratio in xy Direction
- P (Pa): Pressure
- ρ (kg/m^3): Density
- Θ (degrees): Fiber Orientation Angle
- T (^{o}K): Temperature
- T_∞ (^{o}K): Fluid Temperature
- $T_S(^{o}K)$ Surface Temperature

8.0 REPORT FROM S. MCNEILL

Final Report

From

Stephen R. McNeill

On Work Performed at
NASA's NonDestructive Evaluation Branch
During Summer of 92

August 14, 1992

Stephen R. McNeill
Dept. of Mechanical Engineering
University of South Carolina
Columbia SC, 29208
(803)777-3407

Final Report

INTRODUCTION

This report is on the activities performed by Stephen R. McNeill under the direction of NASA's Marshall Space Flight Center Non-Destructive Evaluation Branch (EH-13) branch personal Sam Russell during the summer of 1992. The areas of activities included evaluation of the Shearography system for computer analysis, continuation of development of a PC based 2-D image correlation system, testing and evaluation of the 2-D image correlation program, and the study of the feasibility of using USC's 3-D profile image correlation system at remote sites. The work was performed under a subcontract with the University of Alabama, Huntsville. Dr. Workman was the contract monitor.

SHEAROGRAPHY

NASA's EH-13 has obtained a custom built shearography system for the use in non-destructive evaluation of items of interest to NASA. The system was built by Pratt and Whitney Corp and is currently operated by Pratt and Whitney's Tom King. Tom King indicates that he was the designer of the system.

The system is a digital system which means the images produced are a manipulation of images captured using digitized video. The system initially captures a sheared image of an object which is illuminated with light from a laser so as to cause the formation of constructive/destructive speckles. A driving force is then applied to the object of interest and phase shifted images are captured in rapid succession. These images are then manipulated by an image processing system to produce a continuous set of output images. If one watches the images as they appear on the video monitor a set of "traveling" fringes can be seen. The interpretation of the these fringes can be used in the determination of a parts integrity.

The initial thought was to capture the fringes which are typically available from shearography systems and automatically interpret them for input into numerical models. The system in its current configuration does not have the capability to produce the fringes needed to accomplish this task. Tom King indicated that it might be possible to re-program the system to produce the desired fringes.

The system as designed appears to be a good system for finding flaws, which is what it was designed to do, but does not appear to have the capacity to produce the images needed to get data that can be used as input to a numerical scheme.

A study was performed to see if the shearing head could be used to obtain images needed for input to the program developed by the University of South Carolina's Department of Mechanical Engineering for 3-D profiling using image correlation. This technique would require the separation of the sheared image into two separate images. Several methods were looked at with none having the ability desired. It was decided that in the current configuration that it may not be possible to use the shearography head for this purpose.

PC BASED 2-D IMAGE CORRELATION PROGRAM

This work consisted of upgrades to the program developed by S.R.McNeill Services under contract to NASA during the summer of 91. The program was improved to make the

Newton-Raphson technique robust, a technique was added which requires less memory then the other correlation methods available, a section was added to improve data presentation, and capabilities were programmed to allow the output of images and data contours to standard Windows programs so they can be printed. Floppy disk containing the program and executable code was given to Sam Russell. Copies were also left of the 386 and 486 computer located in building 4702 in the UT lab.

Improvements to Newton Raphson

The section of Newton Raphson section of the program was completely rewritten. Previously the program determined the needed first and second derivatives of the correlation function using a discrete method. The new program uses analytical derivatives. This change boosted the CPU performance by an order of magnitude and seemed to add some stability to the finding of displacements and displacement gradients.

Because the technique is based on the determination of six parameters which minimizes a non-linear equation, there is sometimes problems with the solution getting "lost". To increase the robustness of the algorithm, sections were added to help find proper guesses for the start of the Newton-Raphson technique. These decisions are based on the value of the first derivative of the correlation function as well as the overall correlation value. The values chosen were normalize on the subset size.

These changes have appeared to greatly improved the speed and utility of this technique. For "good" images the speed for looking at 15*15 points appears to be about 15 minutes on a 486 33Mhz computer. There is no set time for how long it will take the program to do a correlation using this technique because of the variability built into the program to handle different situations as they arise.

Section for Less Memory

The program if run in the Coarse-Fine Search or Newton-Raphson mode has a minimum memory requirement of 3 MBytes while running. In some situations on some computers this may be prohibitive. So a new way of running the Coarse-Fine Search Method was devised. The method give results which are identical to the Coarse-Fine Method

The method reformulated the bilinear interpolation function so as not to require the four factors which are normally used, instead the actual gray levels are used. By doing this the storage required to store the bilinear interpolation factors is eliminated thereby saving 2MByte of memory storage. Also these factors do not have to be precalculated as they are now. The down side is that each interpolated gray value need is determined using a equation which requires four more multiplications. For a single point interpolation using a 20 by 20 subset that translates into 4,800 more multiplications at best. It appears that on a 486 33Mhz computer that this translates into a 3 second increase in the CPU time per point. 30 seconds is saved by not precalculation the interpolation factor therefore the break even point on CPU time is reached when 10 points are correlated.

Graphical Display of Correlation Results

Typical correlation runs determine the u and v displacements and four displacement gradients for over 200 image points. This amount of data typically must be interpreted by the

experimentalist. Do to the large amounts of data generated graphical means are most often employed. In the past the data in the output ASCII file was loaded into third party software packages, such as Surfer, and presented for interpretation. To help the experimentalist visualize the data faster two graphical presentation of the results is now possible using the correlation program. Either method can be selected and files from previous correlation runs can be displayed. The user can selected which data field is to be displayed.

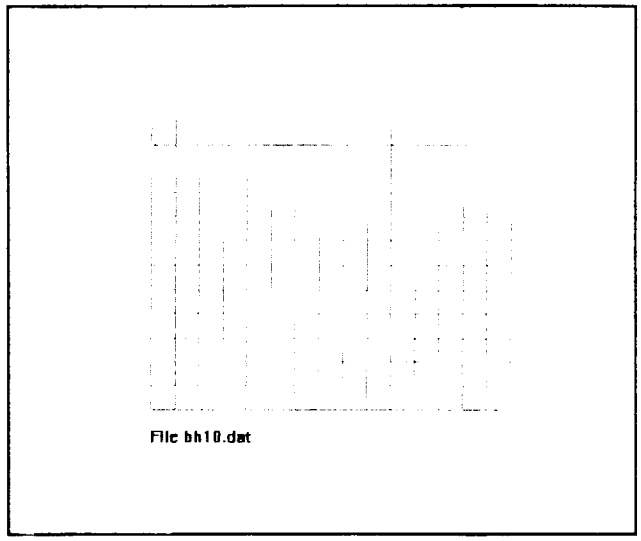

Figure 1: Grid from correlation program

The first method presents the data as a deformed grid. That is the position and the u and v displacements are read from a correlation file. A undeformed grid is first presented on the PC monitor which represents all the points correlated then a deformed grid is drawn which shows how the points displaced. The grids can also be superimposed on a displayed image. The image of the grid (or image with grid) can be saved to a bitmap file which can then be imported into a program such as Windows's PaintBrush and printed. A Sample of the output is shown in Figure 1.

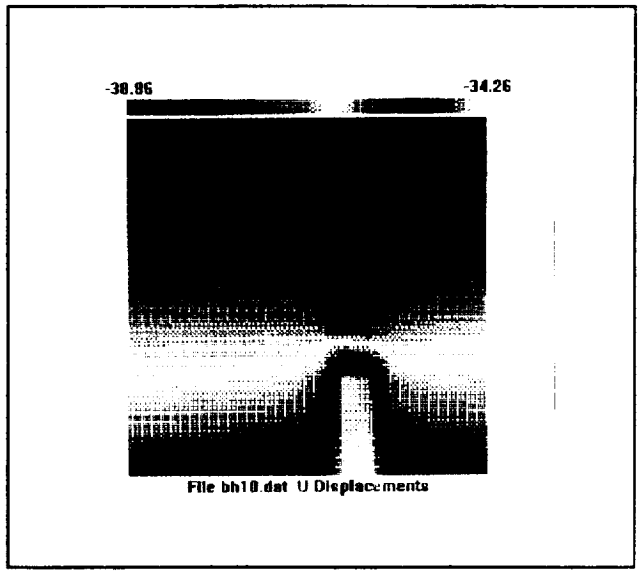

Figure 2: Contours from correlation program

The second method presents the data as a set of color contours. The desired data field is read from a correlation file and analyzed. A continuous color contour map is displayed. The area between data points is filed with color according to a bilinear interpolation scheme. The contour can be saved to a bitmap file which can then be imported into a program such as Window's PaintBrush and printed. A Sample of the output is shown in Figure 2.

Building of Help Files

To facilitate the use of the correlation program, a program for online help was created. The program was built using MicroSoft's SDK help generator. The input to the generator is Rich Text Format file. For this work this file was created using Microsoft's Word for Windows. A floppy disk containing these files was delivered to Sam Russell.

2-D IMAGE CORRELATION TEST

Test Performed

Several correlation test were run during the summer. The purpose of the test were to explore the uses of the image correlation program, test its capability, and demonstrate its utility. The test were run at various facilities at Marshal Space Flight Center. A large number of images were obtained and analyzed. Images and data are not included in this report do to the large volume of images and data. The files containing the images and data are shown in the tables all files refer to the hard disk on the 486 computer in building 4702's UT lab.

May 21, 1992:

This test was run using samples prepared by NASA's Allen Nettles. The specimens were composite specimens which were 8-ply graphite epoxy specimens. The specimens layup and material were T300-934 $(0_2, 90_2)_s$. Three specimens were loaded in tension until failure. Listed below is the image name and load at which the image was obtained. The magnification images are RH.IMG and RV.IMG. All images can be found in directory c:\mcneill\may2192

Specimen #1: Undamged with no holes.

Image Name	Load (lbs)	Notes
NH0.IMG	800	
NH1.IMG	1,000	
NH2.IMG	2,000	
NH3.IMG	3,000	
NH4.IMG	4,000	Cracking Sounds begin
NH5.IMG	5,000	
NH6.IMG	6,000	
NH7.IMG	7,000	
NH8.IMG	8,000	
NH9.IMG	9,000	
NH10.IMG	10,000	
NH11.IMG	11,000	
NH12.IMG	12,000	
NH13.IMG	13,000	Failure at 13,300 lbs.

Specimen #2: With hole drilled to specs.

Specimen #2: With hole drilled to specs.

Image Name	Load (lbs)	Notes
GH0.IMG	400	
GH1.IMG	1,000	
GH2.IMG	2,000	
GH3.IMG	3,000	
GH4.IMG	4,000	
GH5.IMG	5,000	Cracking Sounds Begin
GH6.IMG	6,000	Sounds of Fibers Popping
GH7.IMG	7,000	
GH8.IMG	8,000	
GH9.IMG	9,000	
GH10.IMG	10,000	
GH11.IMG	11,000	Fibers pop and dust is seen
GH12.IMG	12,000	
GH13.IMG	13,000	
GH14.IMG	14,000	Failure at 14,600 lbs

Specimen #3: With hole not drilled to specs.

Image Name	Load (lbs)	Notes
BH0.IMG	400	
BH1.IMG	1,000	
BH2.IMG	2,000	
BH3.IMG	3,000	Cracking Sounds begin
BH4.IMG	4,000	
BH5.IMG	5,000	Loud Popping Sounds
BH6.IMG	6,000	
BH7.IMG	7,000	
BH8.IMG	8,000	
BH9.IMG	9,000	
BH10.IMG	10,000	Loud Pop, fibers separating toward edges.
BH11.IMG	11,000	No fibers coming out
BH12.IMG	12,000	Fibers popping loudly, fibers sticking out
BH13.IMG	13,000	Failure at 13,000 lbs.

July 10, 1992

This test was run using samples prepared by NASA's Allen Nettles. The specimens were composite specimens which were 8-ply graphite epoxy. The specimens layup and material were T300-934 $(0, 45_2, 90)_2$. Four specimens were loaded in tension. The maximum load applied was well below what the failure load was thought to be. After images were obtained, the specimens were unloaded and NDE inspection were performed. Both Radiography and Ultrasonics NDE inspection were performed. The idea was to see if image correlation could be used to find the damage zones. Listed are the image names and the load at which the images were obtained. Images are located in directory c:\mcneill\jul1092.

Specimen #1: Heavy impact (1.3 ft-lb_f). Specimen dimension 2.335" by 0.040".

Image Name	Load(lbs)	Notes
RULE1.IMG		Magnification image
A0.IMG	70	
A1.IMG	500	
A2.IMG	1,000	
A3.IMG	1,500	
A4.IMG	2,000	

Specimen #2: Light impact (0.63 ft-lb_f). Specimen dimension 2.341" by 0.040".

Image Name	Load(lbs)	Notes
RULE1.IMG		Magnification image
B0.IMG	70	
B1.IMG	500	
B2.IMG	1,000	
B3.IMG	1,500	
B4.IMG	2,000	
B5.IMG	1,970	AE after image 2,000 lb load then loaded dropped.

Specimen #3: Hole drilled to specs. Specimen dimension 2.342" by 0.040".

Image Name	Load(lbs)	Notes
RULE1.IMG		Magnification image
C0.IMG	70	
C1.IMG	500	
C2.IMG	1,000	Acoustic Emission
C3.IMG	1,500	
C4.IMG	2,000	

Specimen #4: Hole not drilled to specs. Specimen dimension 2.344" by 0.040".

Image Name	Load(lbs)	Notes
RULE1.IMG		Magnification image
D0.IMG	70	
D1.IMG	500	
D2.IMG	1,000	Acoustic Emission
D3.IMG	1,500	
D4.IMG	2,000	Acoustic Emission

July 20, 21, and 22, 1992

This test was run using samples prepared by NASA's Allen Nettles and the University of Alabama's Alton Highsmith. The specimens were composite specimens which were fabricated to simulate the casing of a solid rocket motor. The specimens were impacted either with or without a backing which was to simulate the solid rocket fuel. All specimens were loaded until failure. The images of specimens 1,2,3,4, and 5 can be found in c:\mcneill\jul2092. Images of specimens 6, 7, 8, and 9 can be found in c:\mcneill\jul2192. Images of specimens 10, 11, 12, 13, 14, and 15 can be found in c:\mcneill\jul2292.

Specimen #1: Medium impact with backing (7.90 ft-lb_f). 15R failure at 94,800 lbs

Image	Load(lbs)
RULEA.IMG	Magnification
POINTA.IMG	Points to damage
REFA.IMG	5,250
A1.IMG	12,500
A2.IMG	20,000
A3.IMG	30,000
A4.IMG	40,000
A5.IMG	50,000
A6.IMG	60,000
A7.IMG	70,000
A8.IMG	80,000
A9.IMG	90,000

Specimen #2: High impact with backing (12.08 ft-lb_f). 16L failure at 83,000 lbs

Image	Load(lbs)
RULEA.IMG	Magnification
POINTB.IMG	Points to damage
REFB.IMG	5,000
B1.IMG	20,000
B2.IMG	30,000
B3.IMG	40,000
B4.IMG	50,000
B5.IMG	60,000
B6.IMG	70,000
B7.IMG	80,000

Specimen #3: High impact with backing (12.05 ft-lb_f). 20M failure at 93,000 lbs

Image	Load(lbs)
RULEA.IMG	Magnification
POINTC.IMG	Points to damage
REFC.IMG	5,500
C1.IMG	20,000
C2.IMG	30,000
C3.IMG	40,000
C4.IMG	50,000
C5.IMG	60,000
C6.IMG	70,000
C7.IMG	80,000
C8.IMG	90,000

Specimen #4: High impact with backing (12.11 ft-lb_f). 13M failure at 93,000 lbs

Image	Load(lbs)
RULEA.IMG	Magnification
POINTD.IMG	Points to damage
REFD.IMG	4,750
D1.IMG	20,000
D2.IMG	30,000
D3.IMG	40,000
D4.IMG	50,000
D5.IMG	60,000
D6.IMG	70,000
D7.IMG	80,000

Specimen #5: Medium impact with backing (7.64 ft-lb_f). 21L failure at 88,000 lbs

Image	Load(lbs)
RULEA.IMG	Magnification
POINTE.IMG	Points to damage
REFE.IMG	5,000
E1.IMG	20,000
E2.IMG	30,000
E3.IMG	40,000
E4.IMG	50,000
E5.IMG	60,000
E6.IMG	70,000
E7.IMG	80,000

Specimen #6: Medium impact with backing (7.61 ft-lb_f). 22L failure at 88,000 lbs

Image	Load(lbs)
RULEF.IMG	Magnification
POINTF2.IMG	Points to damage
REFF.IMG	4,875
F1.IMG	20,000
F2.IMG	30,000
F3.IMG	40,000
F4.IMG	50,000
F5.IMG	60,000
F6.IMG	70,000
F7.IMG	80,000
F8.IMG	90,000

Specimen #7: Light impact with backing (3.04 ft-lb_f). 12L failure at 100,750 lbs

Image	Load(lbs)
RULEF.IMG	Magnification
POINTG.IMG	Points to damage
REFG.IMG	5,000
G1.IMG	20,000
G2.IMG	30,000
G3.IMG	40,000
G4.IMG	50,000
G5.IMG	60,000
G6.IMG	70,000
G7.IMG	80,000
G8.IMG	90,000
G9.IMG	100,000

Specimen #8: Light impact with backing (2.95 ft-lb_f). 13R failure at 90,350 lbs

Image	Load(lbs)
RULEF.IMG	Magnification
POINTH.IMG	Points to damage
REFH.IMG	5,375
H1.IMG	20,000
H2.IMG	30,000
H3.IMG	40,000
H4.IMG	50,000
H5.IMG	60,000
H6.IMG	70,000
H7.IMG	80,000

Specimen #9: Light impact with backing (3.01 ft-lb_f). 16M failure at 88,750 lbs

Image	Load(lbs)
RULEF.IMG	Magnification
POINTI.IMG	Points to damage
REFI.IMG	5,000
I1.IMG	20,000
I2.IMG	30,000
I3.IMG	40,000
I4.IMG	50,000
I5.IMG	60,000
I6.IMG	70,000
I7.IMG	80,000

Specimen #10:Medium impact without backing (7.41ft-lb_f). 24M failure at 92,375lbs

Image	Load(lbs)
RULEJ.IMG	Magnification
POINTJ.IMG	Points to damage
REFJ.IMG	5,050
J1.IMG	20,000
J2.IMG	30,000
J3.IMG	40,000
J4.IMG	50,000
J5.IMG	60,000
J6.IMG	70,000
J7.IMG	80,000
J8.IMG	90,000

Specimen #11: Medium impact without backing (7.07ft-lb_f). 25R failure at 91,500 lbs

Image	Load(lbs)
RULEJ.IMG	Magnification
POINTK.IMG	Points to damage
REFK.IMG	5,000
K1.IMG	20,000
K2.IMG	30,000
K3.IMG	40,000
K4.IMG	50,000
K5.IMG	60,000
K6.IMG	70,000
K7.IMG	80,000
K8.IMG	90,000

Specimen #12:Heavy impact without backing (12.02 ft-lb_f). 23M failure at 95,000lbs

Image	Load(lbs)
RULEJ.IMG	Magnification
PTL.IMG	Points to damage
REFLA.IMG	5,000
L1.IMG	20,000
L2.IMG	30,000
L3.IMG	40,000
L4.IMG	50,000
L5.IMG	60,000
L6.IMG	70,000
L7.IMG	80,000
L8.IMG	90,000
L8PRIME.IMG	95,000

Specimen #13: Heavy impact without backing (11.85 ft-lb_f). 23L failure at 84,750 lbs

Image	Load(lbs)
RULEJ.IMG	Magnigication
POINTM.IMG	Points to damage
REFM.IMG	5,000
M1.IMG	20,000
M2.IMG	30,000
M3.IMG	40,000
M4.IMG	50,000
M5.IMG	60,000
M6.IMG	70,000
M7.IMG	80,000
M8PRIME.IMG	84,750

Specimen #14: Heavy impact without backing (11.97 ft-lb_f). 24L failure at 82,250 lbs

Image	Load(lbs)
RULEJ.IMG	Magnigication
POINTN.IMG	Points to damage
REFN.IMG	5,020
N1.IMG	20,000
N2.IMG	30,000
N3.IMG	40,000
N4.IMG	50,000
N5.IMG	60,000
N6.IMG	70,000
N7.IMG	80,000

Specimen #15: Medium impact without backing (7.33ft-lb_f). 23R failure at 85,500 lbs

Image	Load(lbs)
RULEJ.IMG	Magnigication
POINTO.IMG	Points to damage
REFO.IMG	5,030
O1.IMG	20,000
O2.IMG	30,000
O3.IMG	40,000
O4.IMG	50,000
O5.IMG	60,000
O6.IMG	70,000
O7.IMG	80,000
O7PRIME.IMG	85,500

Data Analyzed

May 21, 1992

The data files are located on the EH-13's 486 computer located in the UT lab. The files are stored on the hard disk under the sub-directory c:\mcneill\may2192\results. Each image file of a set is correlated with the 0 image. Each data file is saved under the name which is the same as the image correlated with the 0 image with the extension dat. (i.e. gh0.img is correlated with gh5.img and the results are stored in gh5.dat).

All correlation were performed in the row direction with the first column starting at 100 last is 400 in steps of 20. The columns were the same (i.e. 100x400x20). 20 by 20 subsets were used for correlating. The correlation was performed using coarse-fine search.

The data for the no hole specimen should show a uniform varying displacement field with the u displacement varying in the vertical direction and the v displacement varying in the horizontal direction. By viewing the contours and grid display it can be seen that the specimen was loaded so that some shear was introduced into the specimen. The data does show a somewhat linear increase in the displacements as the load increased.

The data for the good and bad hole images show that the zone above and below the hole separates from the rest of the outer layers and in the higher loads is translating with the load grips.

This data was transferred to Jim Yang who is using this data as input into his finite element model of this specimen. Jim hopes to use this data as a means of predicting the onset of failure.

July 10, 1992

The data files are located on the EH-13's 486 computer located in the UT lab. The files are stored on the hard disk under the sub-directory c:\mcneill\jul1092\results. Each image file of a set is correlated with the 0 image. Each data file is saved under the name which is the same as the image correlated with the 0 image with the extension dat. (i.e. c0.img is correlated with c3.img and the results are stored in c3.dat).

All correlation were performed in the row direction with the first column starting at 100 last is 400 in steps of 20. The columns were the same (i.e. 100x400x20). 20 by 20 subsets were used for correlating. The correlation was performed using the Newton-Raphson search method.

The data for the A specimen (the specimen for heavy impact) shows similar fiber pull out seen above and below the hole on the hole specimen. The affect of the impact is visible at the lowest of loads. X-ray and UT scans of the specimen also show the size of the impact.

The data for the B specimen (the specimen for light impact) shows little affect of the impact. Even at the highest load of this test, one would be hard pressed to reliably tell if damage was present. The x-ray scan of the specimen after testing shows very little damage although some evidence of damage can be seen. The UT scan of the specimen indicated a damage zone which is much smaller then that of the heavy impact damage but present none the less.

The data for the C and D specimen shows similar results seen for the May21 data at low loads. This data was also give to Jim Yang for analysis. For the C specimen he used this data to predicted the first fiber failure and got a value which was extremely close to the first pop that was heard. Unfortunately the acoustic emission from the specimens were not carefully recorded. His results do indicated that when combined with image correlation a correction to the finite element solution may yield truer results then finite elements used with an assumed boundary condition.

July 20, 21, 22, 1992

The data files are located on the EH-13's 486 computer located in the UT lab. The files are stored on the hard disk under the sub-directory c:\mcneill\jul2092\results. Each image file of a set is correlated with the REF image. Each data file is saved under the name which is the same as the image correlated with the REF image with the extension dat. (i.e. REFB.img is correlated with b3.img and the results are stored in b3.dat).

All correlation were performed in the row direction with the first column starting at either 100, 120, 140 or 160 depending on the amount of displacement. The last row is 400 in steps of 20. The columns were the same as in the previous test (i.e. 100x400x20). 30 by 30 subsets were used for correlating. The correlation was performed using the Newton-Raphson search method.

Not all the images have been correlated at this time. Images not correlated will be correlated at USC and results transferred back to Sam Russell. Of the data that has been analyzed it appears to have the same type of trends that was seen in the previous impact data. At low impact loads little of no evidence of damage is seen at the higher impact loads evidence of damage is seen.

Once the images are correlated they will be compared to the breaking loads to see if a the evidence of damage as seen by correlation can be used to predict the amount of damage sustained by the specimen and the corresponding loss in strength.

3-D PROFILE IMAGE CORRELATION

Test #1

A test was run to test the feasibility of using the 3-D profile image correlation programs at USC on test run at remote sites. The camera and projector used in this system were setup in the shearography lab at Marshal and the needed images obtained. All images were recorded on floppy disk and carried to USC. There the images were analyzed using the programs needed.

The results show that it is possible to perform the test desired. The camera calibration scheme work well and results were as expected.

Test #2

Several test were run at Marshall to determine the affects of post curing on composite plates. Several composite plates were obtained from John Cranston. These specimens were placed in an oven and heated to 250° F. After a soak time the specimens were removed from the oven and placed in proper position to obtain the needed images. Also a external tank faring was subjected to the same process.

The data for these test is currently being analyzed at US. One problem was noted in that the camera/projector setup was vertical during these test and in all previous test they have been horizontal. Although this should not be a problem it did lead to some difficulties in getting the initial guess for the camera calibration routines. Once the data is analyzed the results will be forwarded to Sam Russell.

SUMMARY

As I hope is evident by this report, this summer activities has covered a wide range of topics. The image correlation program has been improved to a point where it could be released to the general experimental community. Sam and I will work this fall to get together the needed documentation to submit the program to NASA's COSMIC program. The image correlation test has yielded a lot of data which is still being digested. It appears that the data will bear out the contention that under certain conditions the image correlation process can be used as NDE tool, although more work needs to be done in this area. The remote 3-D profile seems to be viable but it would be nice if the programs involved could be incorporated into a PC program.